2013

A rheology model of soft elastomeric capacitor for Weigh-in-motion application

Venkata Dharmateja Kollipara
Iowa State University

A rheology model of soft elastomeric capacitor for Weigh-In-Motion application

by

Venkata Dharmateja Kollipara

A thesis submitted to the graduate faculty

in partial fulfillment of the requirements for the degree of

MASTER OF SCIENCE

Major: Civil Engineering (Structural Engineering)

Program of Study Committee:
Simon Laflamme, Major Professor
Brent Phares
Chris Williams

Iowa State University

Ames, Iowa

2013

TABLE OF CONTENTS

Page

LIST OF FIGURES iv

LIST OF TABLES vi

ACKNOWLEDGEMENTS vii

ABSTRACT viii

CHAPTER 1.MOTIVATIONS 1

1.1 WHY WE NEED WEIGH-IN-MOTION 2

1.2 PROBLEM STATEMENT 4

1.3 SCOPE AND OBJECTIVES OF RESEARCH 5

1.4 ORGANIZATION OF THESIS 6

CHAPTER 2.LITERATURE REVIEW 7

2.1 WEIGH-IN-MOTION SENSING (WIM) 7

2.1.1 Sensor Hardware 9

2.1.1.1 Load cell WIM 9

2.1.1.2 Bending plate WIM 10

2.1.1.3 Piezoelectric WIM 11

2.1.1.4 Fiber optic WIM 13

2.1.1.5 Capacitive mat WIM 14

2.1.2 Algorithms 15

2.2 WIM SYSTEM ECONOMICS 16

2.3 APPLICATIONS AND CHALLENGES 18

2.4 CONCLUSION 19

CHAPTER 3.Soft Elastomeric Capacitor 20

3.1 THEORY OF CAPACITIVE SENSING 20

3.2 CAPABILITIES OF SEC 23

3.3 ADVANTAGES 24
3.4 CONCLUSION 24

CHAPTER 4.Constitutive Modeling of Polymers 26

4.1 ZENER MODEL / STANDARD LINEAR SOLID MODEL 29
4.2 PROPOSED MODEL STRUCTURE 31

CHAPTER 5.MECHANICAL BEHAVIOR OF SEC 32

5.1 SPAN OF LOADING 34
5.2 PRELOADING AND MULLINS EFFECT 36
5.3 MULTI-STEP RELAXATION TESTS (MSR TESTS) 37
5.4 SIMPLE RELAXATION TESTS (SR TESTS) 39
5.5 CYCLIC COMPRESSION TESTS (CC TESTS) 41
5.6 PARAMETER EVALUATION APPROACH 43

CHAPTER 6.RHEOLOGY MODEL 44

6.1 EQUILIBRIUM RESPONSE 44
6.2 INSTANTANEOUS RESPONSE 47
6.3 VISCOSITY PARAMETERS 48

CHAPTER 7.NUMERICAL SIMULATIONS AND DISCUSSIONS 52

7.1 DERIVING THE STRESS EQUATION 52
7.2 SIMULATIONS 54
7.2.1 Cyclic compression tests 54
7.2.2 Relaxation tests 57
7.3 IMPACT OF THE PATCH STIFFNESS 59

CHAPTER 8.CONCLUSIONS 63

8.1 APPLICATIONS 64
8.2 SCOPE FOR FURTHER RESEARCH 64

REFERENCES 66

LIST OF FIGURES

Figure 1-1 : Soft Elastomeric Capacitor (Laflamme, Kollosche and Kollipara, et al. 2012) .. 4
Figure 2-1: Single load cell sensor (a) SSPC load cell.
(adapted from wimsystems.com) (b) Installation of load cell. (Fairbanks scales) 10
Figure 2-2: Bending plate WIM sensor. (IRD, Inc.)..... 10
Figure 2-3: Layout of bending plate or load cell WIM system (FHWA.dot.gov). 11
Figure 2-4: Installation scheme of piezoelectric WIM. (FHWA.dot.gov)..... 12
Figure 2-5: LINEAS Quartz piezoelectric WIM. (IRD, Inc.)..... 13
Figure 2-6: Sketch of Michelson Interferometer. (Chang and Rahul 2010)..... 14
Figure 2-7: Capacitance mat WIM system connected with data acquisition devices.
(Loadometer Corp, Baltimore)..... 15
Figure 3-1: (a) capacitive sensor applied on the monitored surface.
(b) Deformation of the surface resulting in a change in the area of the sensing unit.
(Laflamme, Kollosche, et al. 2010) 21
Figure 3-2 : Schematic of SEC based WIM systems..... 22
Figure 4-1 : Kelvin Solid model & Maxwell Fluid model (left to right). 27
Figure 4-2: Behavior of viscoelastic material. (Amin, Alam and Okui 2002) 29
Figure 4-3 : Zener model / Standard linear solid (SLS) model. 30
Figure 4-4 : Schematic representation of the constitutive model. 31
Figure 5-1 : Servo-hydraulic testing machine UTM – 25..... 32
Figure 5-2 : Schematic of the experimental test set up. 33
Figure 5-3 : Applied strain histories in a MSR test on a flexible patch;
a compressive strain rate of 0.0075 mm/s is held constant at each strain step. 37
Figure 5-4 : Typical MSR test results a) stress history
b) equilibrium strain-strain response. 38
Figure 5-5 : Strain histories applied in simple relaxation tests on thin patch;
compressive strain rate is held constant for each time step. 40
Figure 5-6 : Typical compressive stress histories observed in simple relaxation tests..... 40
Figure 5-7 : Strain histories applied in cyclic compression tests..... 42

Figure 5-8 : Typical stress-strain responses obtained from cyclic tests. 42
Figure 5-9 : Flow chart demonstrating the parameter identification of the rheology model. 43
Figure 6-3 : Identification of parameters – Equilibrium response. 45
Figure 6-4 : Identification of parameters – Instantaneous response. 48
Figure 7-1 : Numerical simulations of cyclic loading data
– Stiffer patch a) strain loading rate – 0.0025 mm/s b) strain loading rate - 0.25 mm/s. 55
Figure 7-2 : Numerical simulations of cyclic loading data
– Flexible patch a) strain loading rate – 0.005 mm/s b) strain loading rate - 0.15 mm/s. 56
Figure 7-3 : Numerical simulations of relaxation test data a) MSR test b) SR tests 58
Figure 7-4 : Comparison of resultant stress response under cyclic
compression loading a) slow loading rate b) moderate loading rate c) high loading rate. 60

LIST OF TABLES

Table 2-1: Initial costs of WIM systems (in 1998 $) 17
Table 2-2: Life cycle maintenance costs of WIM systems (in 1998 $) 17
Table 6-1 : Elastic response parameters of the SEC patches 46
Table 6-2 : Viscosity parameters of the SEC patches 51
Table 7-1: Absolute error in predicted stress response using model – stiff patch 61
Table 7-2 : Absolute error in predicted stress response using model – flexible patch 62

ACKNOWLEDGEMENTS

I wish to express my sincere thanks to my major professor, Dr. Simon Laflamme, for being an excellent mentor, advisor, and role model. He supported me during the tough times and provided the much needed encouragement with his cool, calm nature throughout the present research. I also appreciate Dr. Brent Phares for offering me an opportunity to work on interesting bridge projects that provided the much needed financial assistance in the early days and also for being part of my advisory committee. I would also like to acknowledge Dr. Chris R. Williams for his cooperation to use the laboratory facilities, suggestions in fabricating the experimental setup, and also for being part of my advisory committee.

I am thankful to my family for their moral support, encouragement, and motivation throughout my life. I gratefully acknowledge the help of Dr. Sriram Aaleti for his assistance in my academics. I would like to thank Buddi Konkimalla for being there with me in my ups and downs, and bearing with my emotions throughout. I would also thank my dear friends—Neema, Visa, and Alekhya—for helping me give this thesis a better shape in the end. I also thank Hussam for his assistance by fabricating the required sensors. I extend my thanks to Jake and Ashley for their guidance and help in using the UTM machine. I would like to thank all my friends—Rachana, Teja, Loukya, Rohini, Anirudh, Satish, and Venky—for their companionship and support. I wish them all success in their lives.

Finally, I am thankful to Iowa State University for providing me this great opportunity to become a part of it.

ABSTRACT

As a result of fast growing industry, there is an increase in traffic congestion and deterioration of transportation inventory. Real-time traffic characterisation could be used to amoliorate the efficiency of our transportation system. Weigh-In-Motion (WIM) systems offer the advantages of vehicle classification, speed measurement, in addition to weight measurement while vehicles are moving. In this thesis, state-of-the-art WIM systems are discussed and limitations of current technologies are identified. A Soft Elastomeric Capacitor (SEC) that works as a large scale surface strain gauge is introduced to address the limitations in existing techniques and investigated for its applicability as a WIM sensor. Though the novel SEC has potential advantages, the relationship axial strain –to-stress needs to be modeled to enable its utilization as a WIM sensor. A Zener model is selected and modified by the addition of a slider to characterize the polymer behavior. An overstress approach is used to study the resultant stress-strain response owing to its simplicity and computational benefits. Since the overstress approach is data-driven, an experimental testing scheme is used to identify the model parameters. The tests comprise three types of applied strain loading: multi step relaxation, simple relaxation and cyclic compression. Specimens with varying stiffness are employed for these tests.. Numerical simulations for the cyclic compression loading are presented to assess the model performance. The model is found to be capable of reproducing the experimental data with an absolute maximum error value of 0.085 MPa for slow loading rate tests and 0.175 MPa for high loading rate tests. Comparative studies are completed to investigate the impact of patch stiffness on the mechanical behavior of the soft elastomeric capacitor patches. It is observed that as stiffness decreases, the nonlinearity in stress-strain response increases.

CHAPTER 1. MOTIVATIONS

The United States surface transportation system consists of approximately 3.7 million miles of roads and 503 public transit systems (U.S. Department of Transportation 2002). Rapid development of the U.S. economy led to great progress in the development of highway mileage. As a result of this fast growing industry and commerce, a steep increase of over 25 percent is observed in the demands on the transportation system over the past decade (Davis and Susan 2002). This rapid increase in the number of road miles escalates the congestion levels, thereby demanding an urgent need to increase transportation capacity. The capacity can be enhanced by increasing the number of road miles or by developing alternative ways to increase the efficiency of the system.

Intense competition among the leading companies in the supply-chain sector and various transportation modes has increased the number of fully to overloaded trucks and also the gross weights of recently designed vehicles by the automotive companies. A study done by Wang and Li has shown that there are large numbers of vehicles illegally, heavily loaded, exceeding the weight limits (Wang and Liu 2000). Studies show that nowadays trucks are monitored for overload only every ten years, although the truck is in use daily (Jacob and Beaumelle 2010). These overweight vehicles cause damage to the transportation infrastructure. In addition, overweight vehicles cause socio-economic impact due to loss of regulation fees and increase of disorderness in the transportation system leading to increased number of accidents (Wang and Wu 2004). Furthermore, the life span of roads and bridges will be shortened as the increased structural demand on the bridge elements due to overweight vehicles causes unwanted cracking, leading to deterioration of the bridge decks, accumulation of fatigue damage in steel components due to increased stress demands. (Saber and Roberts 2006) . Increased budgets for damage and repair to bridge inventory are lined up against the limited budgets to aid in maintenance and construction of new bridge infrastructures. The need for a weigh station to monitor the gross static weights of the vehicles is imperative, along with the traffic monitoring and pavement condition evaluation techniques. To develop these strategies,

transportation professionals require continuous data about the loading alongside with bridge and pavement performance.

1.1 Why we need Weigh-In-Motion

Weigh stations are checkpoints along the highways to inspect the vehicular weights. The old traditional weigh stations are equipped with truck scales that require the vehicles to stop. There are various disadvantages associated with these widely used traditional static weighing methods at the weigh stations. Although the measurements of the static weight of vehicles are accurate, it involves construction and maintenance of weigh stations at regular intervals along the highway system, which is very expensive. Also at the weigh stations, though it is practically possible to measure the individual axle weights, It is time consuming and causes inconvenience and delays to the driving traffic, which may also become a cause for accidents on heavily traveled roads. Therefore, there is an impending need to improve the efficiency of the system by building the Intelligent Transportation System (ITS) using sensors, communication, and monitoring technologies, which are more accurate, minimizes traffic disruption and economical. In recent times, there is an increased awareness and usage of advanced technology called Weigh-In-Motion (WIM), which reduces the traffic delays and economic aspects involved with the traditional weigh stations. WIM is the technology to measure the gross static weight of vehicle and individual axle weights, while the vehicles are in motion, using advanced technologies.

WIM technology also offers additional advantages as outlined below.

- *Save on operation costs*: Processing the data recorded by the acquisition systems will not only provide information about the weight of the axles, but also furnish data about the spacing between the axles and speed of the vehicle. This can be used for proper administration and planning. Large volumes of this data recorded over years can prove helpful in completing the traffic studies and designing traffic networks. Currently, a vast amount of investment and significant number of

employees are placed into collection of traffic data. WIM technology can potentially save operation costs incurred by companies involved in the transportation sector.

- *Speed monitoring of vehicles*: This can be very important to the police and maintenance services. This could offer potential savings in the amount of money invested in purchasing additional speed tracking equipment by federal and police departments.
- *Updates to code standards*: Information recorded by the WIM systems serves as a feedback loop to understand the performance of the pavement and bridges (WIM installed on the bridge infrastructure is called Bridge WIM or BWIM). The designers can understand and compare the actual loads on the structure to the design loads considered. This can improve the economics by reducing dimensions of the sections for consideration of future designs, thereby reducing construction costs and material quantities by a significant extent.
- *Structural monitoring*: WIM technologies installed along with other types of sensors like accelerometers, strain gauges can be used as tools for Structural Health Monitoring (SHM). The data collected by the WIM and other sensors collectively enable to detect and progressively evaluate the condition of road pavements and bridges, etc., where the WIM sensors are installed in a timely manner.

The complex interaction of vehicle dynamics with WIM systems is an area of prime concern. These vary, depending on the speed of the vehicle, vehicle suspension, and road characteristics. Many new technologies are developed to determine the weight of vehicles in motion, using sensor technology with improved accuracy and a longer lifespan (European Commission 2001). They include bending plate systems, load cells, fiber-optic sensors, and piezo-electric gauges. Unfortunately, these systems are accurate, but suffer from the high costs of installation and maintenance, along with large volumes of data and difficulties in installation.

1.2 Problem Statement

A novel deployable bio-inspired sensing technology, consisting of Soft Elastomeric Capacitors (SEC) in a matrix array as shown in Figure 1-1, has shown promising results at strain monitoring without compromising structural integrity. Scalability of the solution over a surface due to customizable shapes and sizes is a rare solution to find in other health monitoring techniques (Laflamme, Kollosche, et al. 2010). This thesis discusses the work performed to determine the applicability of SEC as a Weigh-in-motion (WIM) sensor. Preliminary step before monitoring the speed & weight using WIM systems is to characterize the response of the system and calibration. Though this capacitance based polymer is promising, it is novel and requires a mathematical relation to predict the amount of stress that caused the measured change in capacitance. Hence, we need a constitutive model to characterize the response of the polymer that relates the applied stress to the strain in the polymer that is related to the measured differential capacitance. The final objective of this thesis is to develop a rheology model of the polymer for WIM system applications under compressive traffic loads.

Figure 1-1 : Soft Elastomeric Capacitor (Laflamme, Kollosche and Kollipara, et al. 2012)

1.3 Scope and Objectives of Research

Polymer materials can be constitutively modeled to determine their stress-strain interactions and temporal dependencies. The scope of this thesis is primarily to develop a constitutive model for characterizing the response of the proposed sensor under varied external conditions for WIM application in traffic management, weight, and speed enforcement. The constitutive model a mathematical model that describes the response of the polymer under various loadings. It is highly important to associate the strains recorded by the SEC to the loads using a mathematical equation. Data processing algorithms will be developed by making use of these relations, along with due consideration to the dynamic interaction of vehicle with the structure/pavement associated with the SEC to measure the gross static weight and speed of the vehicle traversed over the SEC-based WIM system. The extended further scope is to develop an effective monitoring system for the transportation infrastructure that has the combined capabilities of SHM and WIM systems.

In this thesis a number of SEC with different aspect ratios and stiffness are utilized for conducting the strain controlled, compressive loading tests on a universal-testing machine (UTM-25). A variety of tests are performed to characterize the response of sensors within a possible loading range to simulate actual traffic loading conditions post installation of sensors under asphalt. Several constitutive models, based on spring-dashpot analogy, micro-mechanical approach, and overstress approach are studied. A comparative evaluation of numerical results with the test results is completed to display the efficiency of the rheology model considered over the possible strain range. Algorithms are developed to calculate the applied loading with use of the recorded strain data. The model considered and the harnessed algorithms will be developed further to determine the weight, speed, and location of the vehicle using an array of sensor networks. Finally, the results obtained are utilized to discuss the feasibility and applicability of sensing skin as a WIM sensor in the field.

1.4 Organization of Thesis

The remainder of this thesis is organized as follows.

Chapter 2 summarizes the existing WIM systems and challenges faced by the state-of-the-art systems. Chapter 3 discusses the sensing technology using Soft Elastomeric Capacitor (SEC) and its capabilities. Chapter 4 introduces the currently available constitutive models to describe the mechanical behavior of the polymers. Chapter 5 details the experimental procedure and the tests selected to determine the applicability of the skin as a WIM sensor. Chapter 6 describes a parameter identification scheme that is proposed for evaluating the parameters of spring, slider, and dashpot elements. Chapter 7 compares the results of the model to the experiment data. Finally, Chapter 8 summarizes the research work and conclusions are drawn with a discussion on future work to be undertaken for WIM system development.

CHAPTER 2. LITERATURE REVIEW

To date, many bridge owners for example, Golden Gate Bridge, California and Tacoma Narrows Bridge, Seattle have already installed or are currently in the process of following various ITS technologies to enhance the efficiency of traffic flow, level of comfort to drivers, and bridge operations, such as toll collection, weight, speed enforcement, etc. There are various benefits for extending ITS investments into a broader scenario of SHM applications for both operations and structural health in terms of optimal management of long-span bridges. These advantages will be discussed in the following chapters. The literature provided here discusses SHM followed by the concept of WIM systems. Current practice WIM techniques, installation and calibration, advantages and areas for improvement are discussed. A novel bio-inspired capacitive sensing technique is introduced with a short description of its applicability as a WIM system. An additional literature review is completed on the topic of constitutive modeling of the polymers.

The following section introduces the concept of Weigh-in-motion (WIM) sensing, an integral part of the ITS technologies for operational management of transportation infrastructure, and details about the state-of-the-art techniques adopted currently in various states throughout the United States.

2.1 Weigh-In-Motion Sensing (WIM)

WIM systems have a variety of components. Primary components of the system include accurate weighing devices or sensors, software packages, and hardware for data collection and analysis, and a converter to change the recorded signals into the required data type. WIM systems are classified, based on two criteria, (1) speed of vehicles monitored and (2) installation type. The WIM systems are broadly classified, based on the speed of monitored vehicles as follows:

- Low speed systems (<20 mph) - Provide high level of accuracy needed for weight and speed enforcement by federal agencies and toll collection.
- High speed systems (>20 mph) – Eliminate vehicle disruption, while permitting data from the interested type of vehicles with sufficient accuracy for planning.

WIM systems are also classified, based on the installation of weigh-in-motion components as follows:

- Permanent – WIM systems, that have the monitoring sensors or gauges, and the data acquisition devices located at the same location for a long time, are classified as permanent.
- Semi-Permanent – WIM systems, that have data acquisition systems transferable from one site to another with the monitoring sensors installed in the pavement, are classified as semi-permanent.
- Portable – These WIM systems have both the monitoring sensors and data acquisition equipment transferable between monitoring sites.

There are various types of WIM systems classified into the above three categories currently employed by owners for traffic monitoring. FHWA has completed an extensive review and documented the successful practices of WIM technologies in the USA (CTRE - ISU 1997). The current state-of-the-art WIM systems are explained in the following sections.

Many states in the USA conduct traffic monitoring studies for various reasons, including highway planning and motor vehicle enforcement. WIM is a major tool used to record traffic data. WIM data provides planners with traffic volume, classification data, and also provides equivalent single axle loadings (ESAL) that heavy vehicles place on the transportation infrastructure. WIM systems generally use sensors installed under the pavement to determine the vehicle's characteristics. Intended use of WIM data determines the approach for adoption and resources required to maintain the site over the

anticipated design life. There have been several initiatives in the United States that led to the advancement of WIM systems. ASTM standard specifications E-1318, "Standard specification for Highway Weigh-In-Motion," is the primary specification used in the USA (ASTM International 2009). Bridge WIM, an alternative to the traditional WIM systems, is less sensitive to vehicles' dynamics compared to the traditional system. The current state-of-the-art WIM systems are explained in the following sections.

2.1.1 Sensor Hardware

2.1.1.1 Load cell WIM

A load cell WIM is one of the earliest developed WIM systems classified as a permanent system. These systems can be employed for both high and low speed traffic monitoring. A typical load cell consists of a single load cell sensor with two scales placed perpendicular to the direction of travel to detect an axle weight (right and left sides simultaneously). An inductive loop is placed upstream to alert the system of approaching traffic. Additional inductive loops are placed downstream to detect axle spacing's and vehicle speed, based on the location of the monitoring site. These are durable and among the most accurate techniques of WIM. Thus, they can be utilized for both traffic data collection and enforcement purposes. The major disadvantages for these systems are (1) highly expensive among the available technologies and (2) require high capital and life cycle costs. The average lifetime of load cell systems is around five years. A particular model of load cell sensor and installation procedure for the sensor into pavement is shown in Figure 2-1. A typical layout of the load cell WIM is well demonstrated by CTRE- Iowa State University (CTRE - ISU 1997).

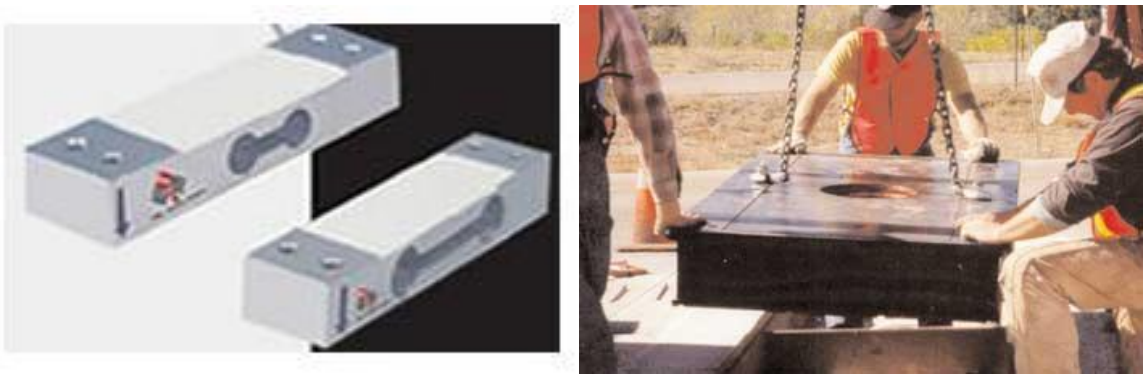

Figure 2-1: Single load cell sensor (a) SSPC load cell. (adapted from wimsystems.com) (b) Installation of load cell. (Fairbanks scales)

2.1.1.2 Bending plate WIM

As the name says, these systems utilize plates with strain gauges attached to the underside of the plate. Strain sensors record the strain data, as the vehicle traverses the plate illustrated in Figure 2-2. Dynamic loads are calculated, using the strain gauge recorded data. This consists of one or two scales placed perpendicular to the traffic flow direction.

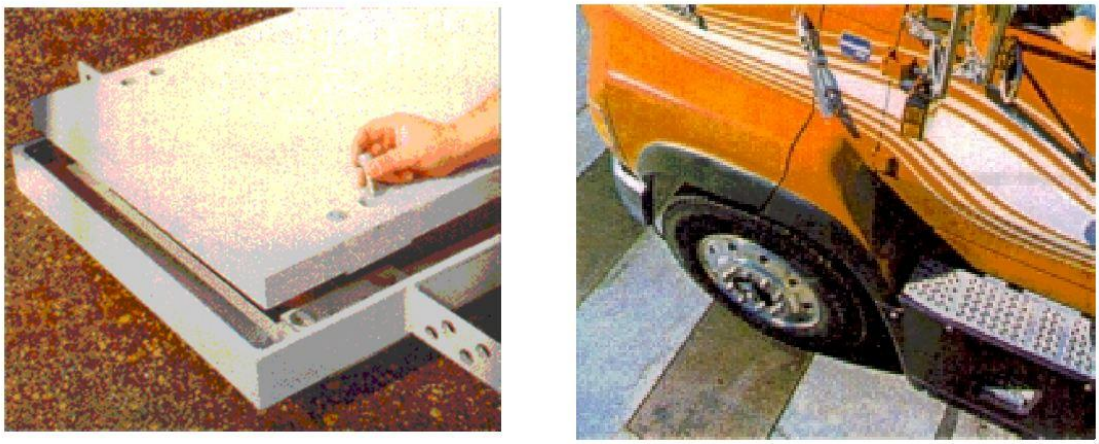

Figure 2-2: Bending plate WIM sensor. (IRD, Inc.)

Bending plate WIM can be portable or permanent type, while the earlier is not a high speed WIM. A bending plate WIM consists of two inductive loops placed upstream and downstream for the same reasons as mentioned in section 2.3.1.1. These systems offer

three possible ways to detect vehicle speed, demonstrated in the typical layout shown in Figure 2-3. These systems can be used for traffic data collection, as well as weight and speed enforcements with higher accuracy than piezoelectric systems (discussed in the next section). They are economical compared to the load cell systems and generally do not require complete replacement after five years. Accuracy of bending plate WIM systems, in comparison to load cell systems, is a major disadvantage.

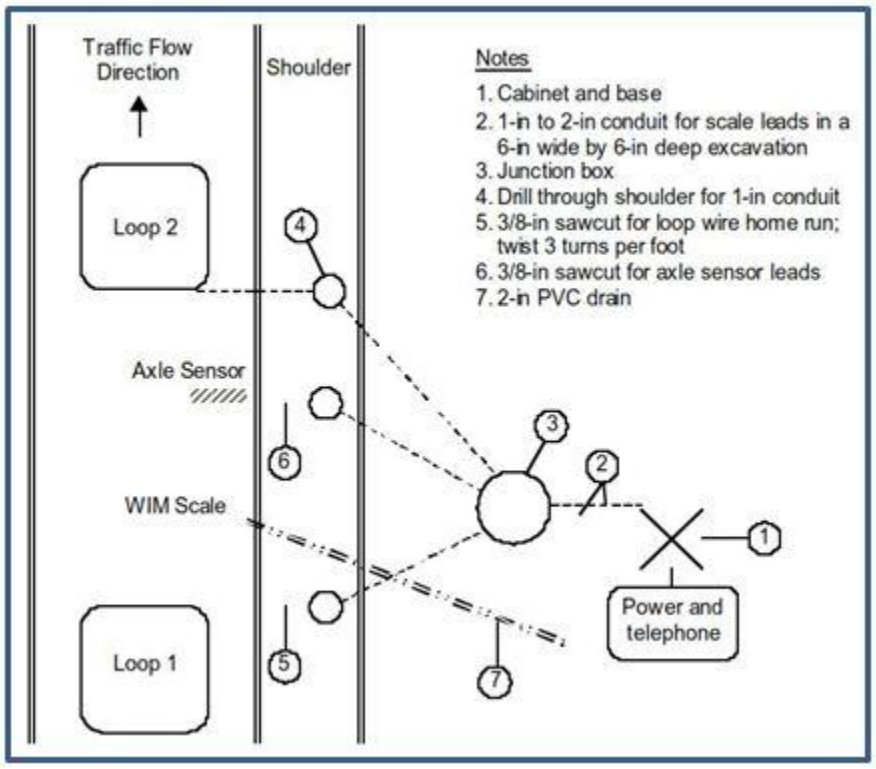

Figure 2-3: Layout of bending plate or load cell WIM system (FHWA.dot.gov).

2.1.1.3 Piezoelectric WIM

Piezoelectric WIM systems consist of piezoelectric sensors that can detect a change in the voltage, due to the pressure exerted by the axle of the vehicle, thereby measuring the weight of the axle. The voltage recorded by the data acquisition system, as the vehicle passes over the piezoelectric system, is used for calculation of dynamic loads. Proper calibration of the system will help calculate static weight of the vehicle. These are the least expensive systems in terms of capital costs and maintenance costs among the WIM

systems currently available. Four lanes can be monitored using piezoelectric systems in comparison with two lanes for load cell WIM and bending plate WIM. They are sufficiently accurate for traffic classification and axle weight determination at speeds up to 60 mph.

The typical system consists of one sensor with two ILDs with the piezoelectric sensor placed perpendicular to the direction of travel and inductive loops placed upstream and downstream. A typical installation of piezoelectric system presented by Luz Elena and Lawrence (2000) in a summary of vehicle detection technologies is shown in Figure 2-4.

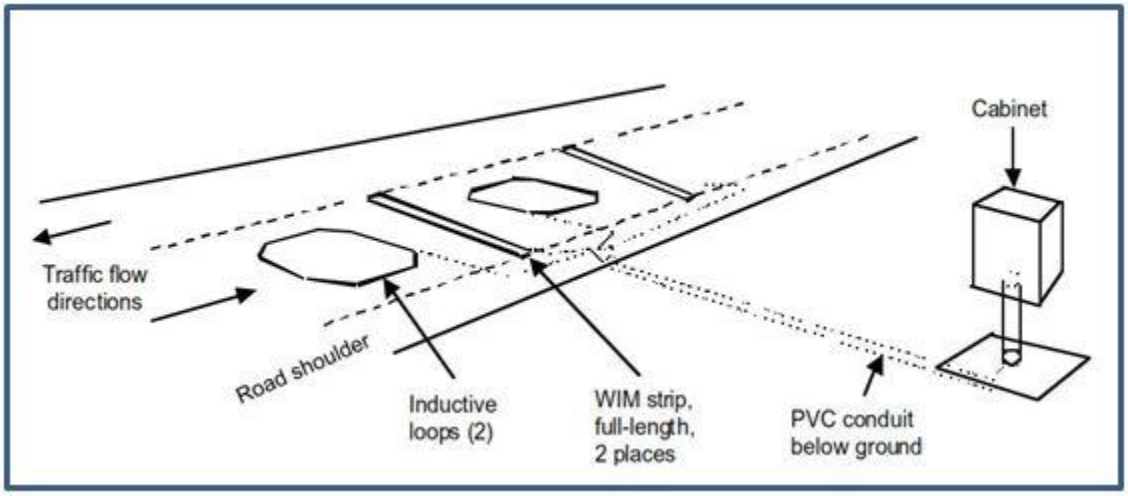

Figure 2-4: Installation scheme of piezoelectric WIM. (FHWA.dot.gov)

Owing to less cost and significant accuracy, extensive research has been completed in the field of piezoelectric WIM. Recent advancements have led to the development of a LINEAS quartz sensor. LINEAS quartz manufactured by Kistler (Kistler Instrumente AG 1997) consists of quartz crystal sensing elements mounted between an aluminum core surrounded by an elastic material as shown in Figure 2-5. One of the areas of concern is the influence of temperature and other environmental conditions on piezoelectric WIM systems, that should be addressed. Also, these systems are highly sensitive to speed variations and must be replaced at least once every 3-4 years.

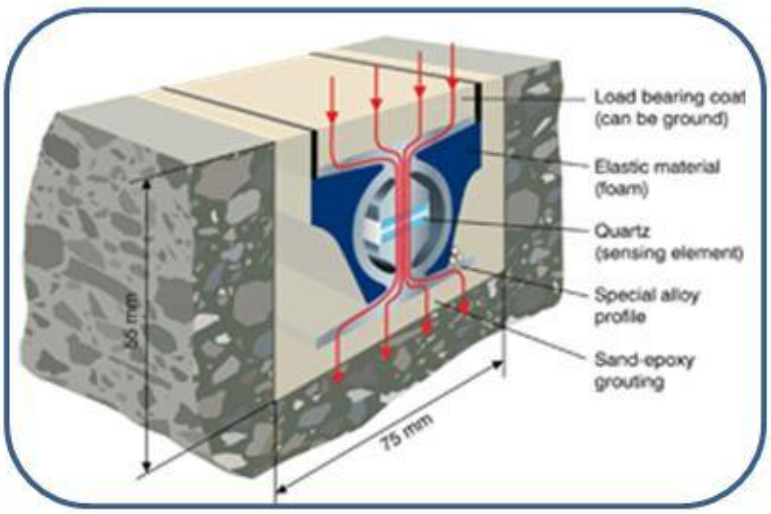

Figure 2-5: LINEAS Quartz piezoelectric WIM. (IRD, Inc.)

2.1.1.4 Fiber optic WIM

Fiber optic sensors employed as SHM systems also have potential capabilities to function as WIM systems. Optical fibers are used to transfer an extensive amount of data in the modern day world. There are various techniques to extract distributed strain and temperature information from optical fibers, like Rayleigh, Raman, and Brillouin scattering. Navarrette and Benabeu (1994) demonstrated the use of fibre optic sensors to measure weigh-in-motion. Chang and Rahul (2010) explained the concepts and principle techniques of fibre optic sensors for infrastructure health monitoring.

The basic principle behind the application of fiber optic WIM is the external pressure acting on the system produces a change in the optical path length detected by a phase change by an interferometer. This change is proportional to stimulus and length of the fiber. A schematic sketch of a Michelson interferometer is shown in Figure 2-6. Fiber optic sensors are currently employed only to measure strain and temperature with high sensitivity and accuracy using distributed sensor networks. Fiber optic sensors can be used as solutions, where electrical gauges for strain and vibration monitoring encounter problems in bias stability. Many researchers are currently working to take advantage of these properties to make an advanced fibre-optic based WIM system.

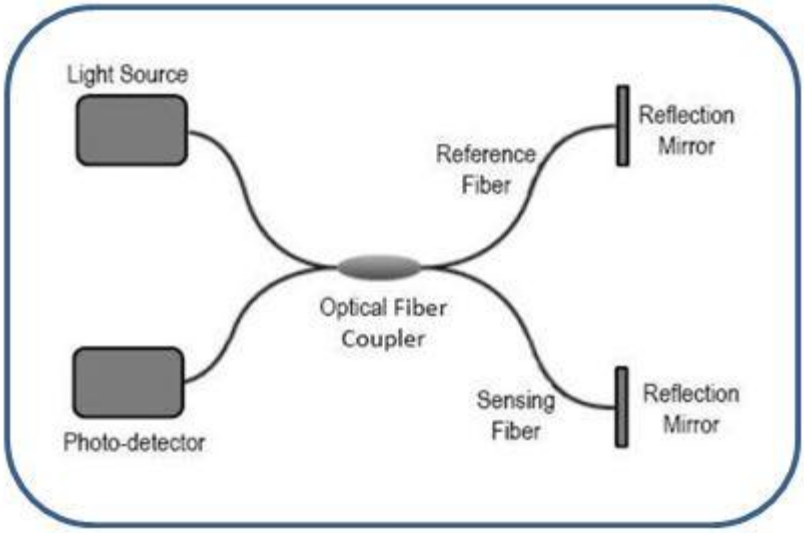

Figure 2-6: Sketch of Michelson Interferometer. (Chang and Rahul 2010)

2.1.1.5 Capacitive mat WIM

Capacitive mat WIM consist of a dielectric material sandwiched between metal steel sheets and voltage is applied across the material sandwich. As the vehicle passes over the mat, spacing between these metal sheets decrease, thus causing the capacitance of the system to increase. The electrical circuit's resonant frequency changes (capacitance mat is a part of it). These changes can be measured by the data acquisition systems. These systems can be classified under both portable and permanent WIM applications capable of monitoring up to four lanes of traffic simultaneously. The capacitance mat systems are among the most expensive WIM systems available at present. The accuracy of these systems is not well compared with the load cell and bending plate WIM systems for estimating axle weights. A photograph of traffic monitoring using the capacitance mat WIM system is shown in Figure 2-7.

Figure 2-7: Capacitance mat WIM system connected with data acquisition devices. (Loadometer Corp, Baltimore)

2.1.2 Algorithms

The concept of weigh-in-motion dates back to the early 1970s (Moses 1979), where the initial WIM system required sensors both on the pavement and beneath the bridge. This was later superseded in Australia with various advancements for use on culverts (Peters 1986). Efforts were made by many researchers for strain based vehicle classification to identify vehicle class, weight, and speed. Wei, Chang, and Wang (1996) used advanced techniques for vehicle classification. Linjun Yan et al. (2008) used neural networks and PCA for strain based classification. Subsequent BWIM methods are based on influence lines. An inverse matrix solution is required to produce individual axle weights. The major setback for this approach is to determine the influence line of in-service bridges, which can be challenging. In 1999, O'Brien et al. (1999) developed a new, simplified approach that only requires a theoretical influence line for bridge WIM. A wide range of field trials has been made in the recent past and new applications continue to emerge. The preliminary approach developed by Moses (1979) used an algorithm to evaluate the sum

of squares of the differences between measurements on bridges to corresponding theoretical strains. Optimization of the estimation errors results in a set of equations involving axle weights. The most advanced technique in those days was the study of Moving Force Identification (MFI). There has been an extensive amount of research to extend this theory into three dimensions. Gonzalez, Rowley, and OBrien (2008) provided a recent advanced solution to the MFI problem by using first order Tikhonov regularization on a bridge plate model.

BWIM methodologies have employed non-intrusive techniques, also termed as Nothing-On the – Road (NOR) sensors. Neural network-based approaches have evolved for classification, based on strain data. Recent testing conducted by Chatterjee et al. (2006) uses a wavelet-based approach to analyze the recorded strain data to produce axle spacing, weight, and vehicle speed. There has been extensive literature explaining the need to determine the weight of moving vehicles. Examples of these include development of a prescreening, bridge rating tool by Nyman and Moses (1985). Swan and Fairfield (2008) installed a BWIM system to monitor the structural condition of the bridge during testing. BWIM has gained momentum around the world. Recent advancements in this field led to the development of SiWIM systems currently employed in less than twenty countries around the world.

2.2 WIM System Economics

The world has seen an increasing number of WIM systems available over last few years with attempts to increase the accuracy and performance at reduced costs. It is more difficult to quantify the accuracy of a WIM system than to determine the accuracy of a static scale. Bushman and Andrew (1998) presented a detailed analysis of the costs and performance of three WIM systems more widely accepted in North America. Economics of WIM systems can be expressed in terms of initial capital costs and life cycle costs. Bergan, Berthelot, and Taylor (1997) completed a study on the effects of WIM accuracy on enforcement, providing economic details of the three technologies used in the USA,

namely piezoelectric WIM, bending plate WIM, and load cell WIM. The budgetary details are tabulated under Table 2-1 and Table 2-2. The life cycle of piezoelectric WIM systems is considered as three years, and bending plate WIM and load cell WIM systems are taken as five years in computing the maintenance costs.

Table 2-1: Initial costs of WIM systems (in 1998 $)

Capital cost component	Piezoelectric	Bending plate	Single Load cell
In-road equipment	$4500	$13000	$34000
Installation labor	$3500	$6500	$10500
Traffic control	$1000 (1 day)	$2000 (2 days)	$4000 (4 days)
Total capital costs	$9000	$21500	$48000

Table 2-2: Life cycle maintenance costs of WIM systems (in 1998 $)

Cost component	Piezoelectric (3 years)	Bending plate (5 years)	Single Load cell (5 years)
In-road equipment	$4000	$6000	$1000
Labor and materials	$4000	$5500	$500
Traffic control	$1500 (1 day)	$1500 (1 day)	$750 (1/2 day)
Total life cycle costs	$9500	$13000	$2250

These figures provide an idea of how various, currently available WIM technologies are placed against each other. They also indicate the costs for improved WIM accuracy and reliability are less, compared to the annual operating budget for an enforcement facility.

2.3 Applications and Challenges

The WIM systems discussed above find their applications under various categories. The potential benefits of the WIM systems are:

- Weight enforcement to avoid performance issues, due to overweight of vehicles
- Speed enforcement for federal agencies
- Toll collection
- Evaluation of permit vehicle models using WIM truck records
- Site specific LRFR factors using WIM data
- Increased level of comfort to users with dynamic motion sensing systems in comparison to static weighing scales.

Despite numerous advantages offered by these WIM systems, there are challenges associated with the use of current technologies. Some of the common challenges for all WIM systems are described below.

- Installation and maintenance of WIM systems in the road surface require pavement cuts or some form of excavation, or some systems require adherence to surface of pavement. Both will require closing down the lanes for traffic use.
- Smoothness of the pavement at the installation site is a critical issue to minimize vehicle dynamics that influence the accuracy of WIM systems.
- Speed of vehicles and individual scale errors also affect the accuracy of the system.
- Vehicle suspension systems, vehicle oscillation and tilting, and brake reaction forces introduce dynamic effects that influence the axle weight determination.

2.4 Conclusion

Scheuter (1997, 1998) has completed a detailed analysis of factors that influence the WIM system's accuracy along with a review of errors and maximum achievable accuracy for a WIM system. There has been an intensive debate in the international front on the importance of physics-based models for identification of systems. To design and implement any system for HM or WIM, the rational approach is to conduct a system-identification and conceptualize the system through a physics-based model using the data obtained. A physics-based model or other models developed would serve as a basis for monitoring changes in the operational parameters of structures and understanding the mechanical behavior of the material or computing the static weight of vehicle using the extracted data.

Recent advancements have led to the development of various new sensing mechanisms/systems like piezoelectric paints, PVDF sensors, and nano PWAS composites, etc. This thesis mainly describes the application of new capactive-based sensing techniques proposed by Laflamme et al. (2010) that is capable of detecting changes in strain at low cost. The following chapter introduces the proposed sensing technique, its mechanism, and discusses its advantages over the above discussed WIM systems.

CHAPTER 3. Soft Elastomeric Capacitor

A novel monitoring technique, termed "sensing skin," includes an array of SEC's (Soft Elastomeric Capacitors) highly sensitive to the changes in strain, acting as a large-scale surface strain gauge. SEC's are composed of a nano-composite layer sandwiched between compliant electrodes. Ease of installation and requirement of less power in comparison with resistance strain gauge allow for application on large surfaces. Its Customizability in shape and size would make it feasible to apply on irregular surfaces unlike other dynamic sensors. Strain on the structures' surface is converted into significant change in capacitance, based on a capacitive sensing technique. A discussion on the theory behind capacitive sensing technique is presented next.

3.1 Theory of capacitive sensing

The sensor unit consists of two highly compliant electrodes separated by a distance, d, with a surface area, A (plan dimension l x b). Compliance is established because of the polymer layer present between the electrodes dependent on the permittivity of the layer. Sensitivity of the sensor unit is directly proportional to the permittivity of the medium between electrodes. The capacitance of the unit is given by:

$$C = \varepsilon_r \varepsilon_o A/d \ . \qquad (3\text{-}1)$$

ε_r and ε_o are the relative permittivity of the material and vacuum permittivity, respectively. Deformation of the capacitive sensor would result in a change of the capacitance as shown pictorially in Figure 3-1. The picture shown below indicates the change in dimension of the SEC along its length while the WIM application will involve a change the dimension along its thickness.

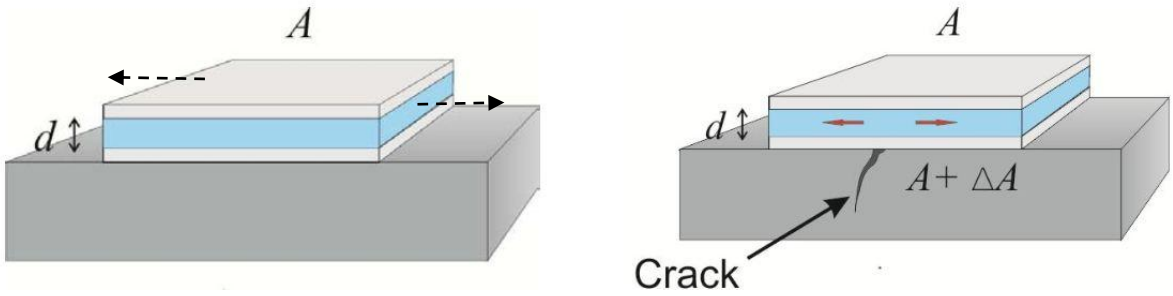

(a) (b)

Figure 3-1: (a) capacitive sensor applied on the monitored surface. (b) Deformation of the surface resulting in a change in the area of the sensing unit. (Laflamme, Kollosche, et al. 2010)

$$C = \varepsilon_r \varepsilon_o \, l*b/d \; . \qquad (3\text{-}2)$$

Change in the capacitance results, due to small changes in the physical dimensions of the sensor, can be calculated by the total differential of the above relation

$$\Delta C = \frac{\partial C}{\partial l}\Delta l + \frac{\partial C}{\partial b}\Delta b + \frac{\partial C}{\partial d}\Delta d \; . \qquad (3\text{-}3)$$

The differential amount of deformation, δb, is negligible and can be ignored.

$$\Delta C = \left(\frac{\Delta l}{l} - \frac{\Delta d}{d} \right) C_{ref} \; . \qquad (3\text{-}4)$$

Using the law of conservation of volume for the initial state and the deformed state, we obtain

$$\frac{\Delta l}{l} = - \frac{\Delta d}{d} \; . \qquad (3\text{-}5)$$

This is equal to strain in the sensor. Thus, the change in capacitance of the soft elastomeric capacitor can be related to the sensor strain, S, as follows

$$S = \frac{\Delta C}{2 * Cref} \quad . \qquad (3\text{-}6)$$

Therefore, the soft elastomeric capacitor sensing system can be modeled as a general expression relating to change in capacitance to change in length as derived in Eq. (3-7).

$$\frac{\Delta C}{\Delta l} = 2\, \varepsilon_r\, \varepsilon_o\, b/d \quad . \qquad (3\text{-}7)$$

This illustrates the sensitivity of the system is inversely dependent on the thickness of the elastomer or directly dependent on the permittivity of the polymer layer.

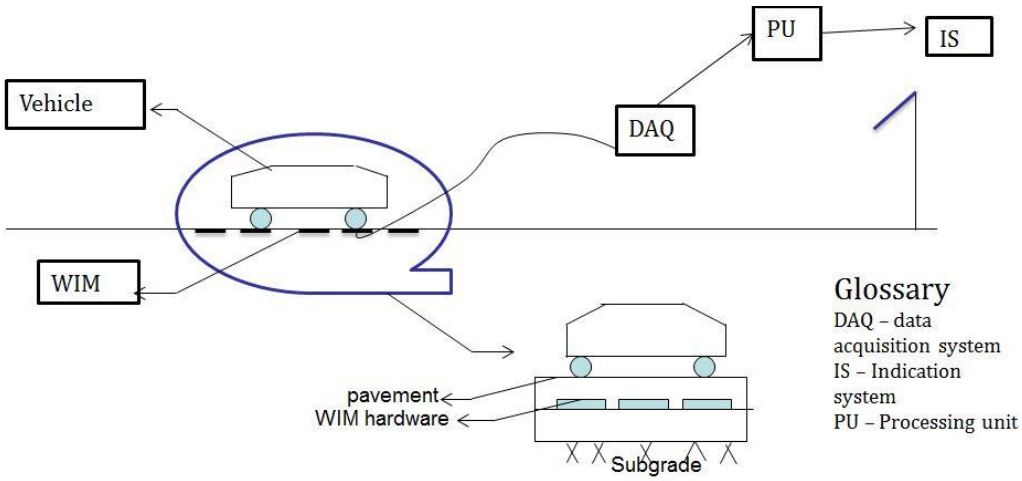

Figure 3-2 : Schematic of SEC based WIM systems

The above application shown in Figure 3-1involves changes in dimension along the length of the SEC patch whereas the WIM application will involve a change in the dimension along the thickness. This will result a change in the capacitance that will be recorded by the data acquisition system. Figure 3-2 presents a schematic of the WIM system indicating the major components associated with the weigh-in-motion. As the vehicle moves over the SEC based WIM system, the thickness of the SEC patch reduces thereby increasing the capacitance of the system. The features recorded by the data acquisition system have to be processed for evaluating the weight and speed of the

vehicle which will be used by the indication system to give a signal to the driver in the vehicle.

3.2 Capabilities of SEC

In the early days, a soft stretchable dielectric polymer with metal film electrodes was demonstrated by Laflamme et al (2010) to be capable of detecting the strain and small surface cracks in reinforced mortar and concrete specimens. Simplicity in the shape of a sensor has been a reason for improved durability. Grafting a conducting polymer to the backbone of the elastomer matrix enhanced the sensitivity of the soft elastomeric capacitor (Kollosche, Stoyanov and Laflamme 2011). Laflamme et.al (2012) increased the robustness of the soft elastomeric capacitor by increasing the thickness of the unit that led to a reduction in basic capacitance adjusted by increasing the permittivity with addition of nanoparticles. The authors demonstrated the self healing capacity of the soft elastomeric capacitor by mechanically-tempering the SEC. Saleem et al. (2012) explained the fabrication procedure of the novel bio sensory membrane composed of a thermoplastic elastomer matrix.

A set of experiments was conducted to demonstrate the capabilities of SEC to detect and localize the cracks over wood and concrete specimens (Laflamme, Kollosche, et al. 2012). Laflamme and colleagues have shown the sensing patch (several SEC's arranged in a matrix) is a promising solution for civil engineering structures by installing the SEC patch on the South Skunk River bridge located in Ames, Iowa. The authors demonstrated its capabilities to detect the dynamic signatures of the bridge and validated them with a steel beam in the lab. By tracking strain histories over 25με, SEC capabilities in condition assessment of civil engineering structures were shown, using a low cost, off the shelf data acquisition system. Possibilities of reconstructing the deflection shapes of civil structures under quasi-static and dynamic loading conditions were demonstrated with a comparable accuracy against the resistance based strain gauges.

3.3 Advantages

There are various advantages of the SEC over the sensing techniques discussed in previous sections. The practical advantages of the SEC that makes the technology directly applicable to civil engineering structures are outlined below.

- Low cost inexpensive materials (SEBS) required for fabricating the SEC. Time and effort required to fabricate SEC patches are relatively less than other sensors.
- Customizable shapes and sizes, coupled with the flexible nature of the SEC, can cover larger areas and critical jointed locations to allow full scale implementation, a vital advantage over other currently available sensors.
- Requirement of low voltage, compared to the resistance-based strain gauges, reduces the operational costs of the WIM system.
- Ease of installation in comparison to WIM systems, like bending plate and fiber optics, etc., not only reduces the initial investment of the system, but also reduces the downtime for traffic.
- Robust in comparison to other WIM systems with respect to physical damage. A damaged patched can still be used for WIM, thereby increasing the life span and reducing the maintenance and replacement costs associated with the system.
- Condition assessment of the structures coupled with WIM could offer potential results to the highway / bridge owners.

3.4 Conclusion

SEC has shown promising results to address the few challenges of WIM systems discussed in Section 2.3. Ease of installation can reduce the downtime of a route for traffic use. The capabilities of SEC to detect the dynamic signatures of civil structures promises improved accuracy against the odds of vehicle dynamics and suspension systems in axle weight measurement of the vehicles. Enhanced sensitivity of the polymer by grafting nano composites can result in accurate detection of strains under dynamic and

static loads that infer the weight and speed of vehicles. A mathematical model for relating the strain in the sensor to the load under varied loading conditions is essential to determine the weight and speed of the vehicles for a SEC-based WIM system. Because the proposed soft elastomeric capacitor is novel, this thesis focuses on developing a rheology model to determine resultant stress response and temporal dependencies. The following chapter presents a brief review of currently available modeling techniques for modeling the stress-strain interaction and their time dependencies of the polymers.

CHAPTER 4. Constitutive Modeling of Polymers

Soft elastomeric capacitors fabricated using Styrene Ethylene Butylene Styrene (SEBS)-based nano composite, using ultrasonic probe/ high-shear mixing methods is classified as a thermoplastic elastomer (Saleem, et al. 2012). Thermoplastic elastomers are classified to have secondary links among the chains that can be stretched repeatedly to a strain of over 200% with an ability to relax to original length when stress is released. The SECs classified as thermoplastic elastomers have various enhanced properties, advantageous for their application as a WIM system, such as friction and wear, less amount of creep, resistance to corrosion, and environmental stress cracking (Brinson and Brinson 2008). Polymeric materials exhibit a behavior between that for elastic solids and viscous liquids, termed viscoelasticity. The complexity of mechanical behavior of thermoplastic elastomers necessitates the requirement for a comprehensive model that can reproduce strain rate dependency, cyclic softening, recovery at zero stress, etc.

Any polymer can be physically described using a constitutive model to explain the time dependent behavior and interaction of stress—strain that occurs in polymers. Viscoelastic behavior is represented by a linear combination of 'springs- elastic component' and 'dashpots- viscous component'. Elastic spring is an analog of Hookean elastic bar, while the damper/dashpot is an analog for Newtonian viscous fluids. There are numerous mechanical models available, based on the various linear combinations of spring and dashpots. Brinson and Brinson (2008) explain the complex models that describe the behavior of polymers over complete history of use. These constitutive models can be equivalently modeled as electrical circuits for better understanding of the engineers, where the spring replicates a capacitor (energy storage) and damper replicates resistor (energy dissipater). Early models, like Kelvin and Maxwell, combine a linear spring with a viscous damper in parallel and series, respectively, as shown in Figure 4-1. The Kelvin model is referred as a solid because it reacts instantaneously and restores its original configuration upon unloading; whereas, the Maxwell model is referred as a fluid because it involve dashpots at initial loading and do not recover completely upon unloading.

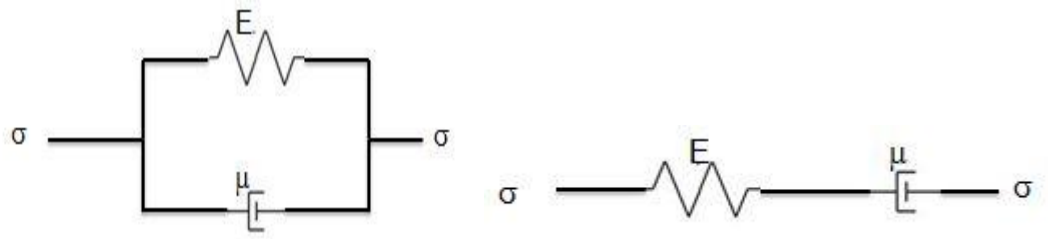

Figure 4-1 : Kelvin Solid model & Maxwell Fluid model (left to right).

The above-defined ones are simple two—element models. A better description of mechanical behavior of polymers is possible by using a minimum of three-element models. There are four possible three-element models, which involve a parallel combination of Maxwell fluid model with spring and damper, respectively, and a series of combinations of Kelvin solid model with spring and damper, respectively. Brinson and Brinson (2008) detailed the procedure to derive the governing constitutive relations for all the above-described models using the physical relations. Strain rate and temperature are two key parameters that significantly influence the mechanical behavior of polymers. Arruda, Boyce, and Jayachandran (1995) studied the effects of strain rate and temperature on finite strain deformation of polymers. The influence of temperature and strain rate on deformation response of various polymers was studied by Blumenthal and Cady (2002), and Richeton et. al (2005) completed extensive studies and experimentation.

Conventionally, two approaches are used to develop stress-strain relations for the polymers. The first approach is based on the phenomenological approach using the modeling theory as described above. The second approach is based on micromechanical modeling, which treats the elastomers as a network of long chains, involved with the molecular level chemistry of the polymeric chains. Boyce and Arruda (2000) mention the main shortcomings of the latter approach in recent surveys on rubbery polymers . They include poor agreement with experimental data and fundamental difficulties under cyclic loading. Another disadvantage from the viewpoint of its applicability to a WIM system is the complicacy involved with the chemistry of the polymers to determine free energies,

entropies and enthalpies, of the elastomer. Time dependence of the elastomers results in numerous experimentally-observed phenomena as described below.

- Rate dependence of monotonic stress-strain behavior.
- Stress relaxation till the elastomer reaches a strain-dependent equilibrium.
- Hysteresis during cyclic loading and its high dependency on the strain rate.

These phenomenon have been extensively studied experimentally and also in the development of finite strain constitutive models over the past few decades. Understanding the behavior of polymeric materials under various types of loading is essential for developing the constitutive model. Detailed information about the influence of temperature and strain rate is required for a fully functional constitutive model in all regimes. Boyce, Socrate and Llana (2000), Bardenhagen, Stout, and Gray (1997), Khan and Zhang (2001), Krempl and Khan (2003), and Drozdov and Christiansen (2003) have developed various constitutive equations over the past to explain the rate-dependent behavior of the polymers. Other famous researchers like Yeoh (1993) ,Mooney (1940) and Rivlin (1951), have developed models based on the theory of hyper elasticity for simulating the behavior of polymers, elastomers, and rubber-like materials. Bergstom (2003) reviewed the current state-of-the-art constitutive models for their predictive capabilities in simulating the behavior of filled elastomers.

These earlier proposed models are complicated to precisely model the stress-strain interaction and temporal dependencies of the polymer. Owing to difficulty in inverting the model limits the applicability of these models for a WIM system or condition assessment of the pavement or the bridge structure. Simpler, but effective, models that can predict the behavior of polymers have been proposed. Several models were studied for modeling the nonlinear stress-strain response of the SEC and a typical three-parameter model known as the Zener model is chosen over the other available models.

4.1 Zener model / Standard linear solid model

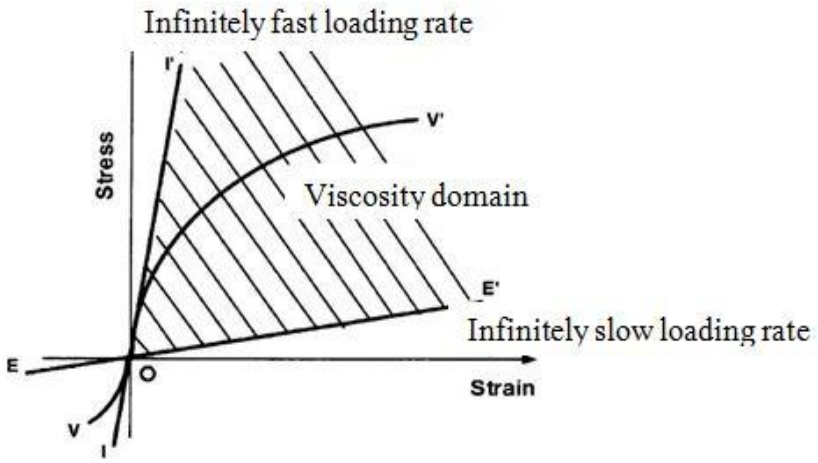

Figure 4-2: Behavior of viscoelastic material. (Amin, Alam and Okui 2002)

A typical schematic representation of the rate-dependent response of the viscoelastic solid is shown in Figure 4-2. Viscosity domain is bounded by the instantaneous response under an infinitely fast rate of loading and equilibrium response under infinitely slow rate of loading. A phenomenological model that can meaningfully express the instantaneous and equilibrium response can be considered. With a limitation of applicability of the model for a WIM system, a simple three-parameter model, based on the overstress approach can be effective. In a three-parameter model, termed as Zener or Standard linear solid (SLS) model (see Figure 4-3), the first branch consists of a spring to explain the equilibrium response, while the other branch with a spring and dashpot explains the "overstress" caused by the rate dependent effects. Bhuiyan et al. (2009) employed similar models to physically model the response of rubber bearings in a seismic base isolation technique. Nonlinear spring and dashpot elements might be required in addition to the linear springs to represent the nonlinear equilibrium and instantaneous responses obtained from the SECs. Comparative performance evaluations of the SLS model against the standard constitutively developed models like Yeoh (1993), Berger-Boyce (2001), Mooney (1940), Rivlin (1951), and Arruda-Boyce (2000) were conducted by Amin to

determine the viscoelastic response of natural and high damping rubbers (Amin, Alam and Okui 2002). The capabilities of the model to simulate the response of the rubber are well depicted.

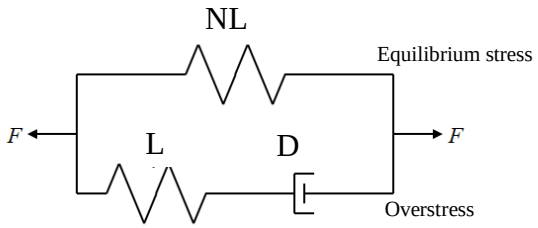

Figure 4-3 : Zener model / Standard linear solid (SLS) model.

This three-element standard solid model with a spring in parallel to a Maxwell element was shown to predict the response of the polymers effectively under various loading conditions at different temperatures by Amin et al. (2002). In this model the branch with spring 'NL' represents the path-dependent equilibrium stress, while the second branch with Maxwell element represents the rate dependent overstress. A three-dimensional framework of the SLS model proposed by Bergstrom and Boyce (2001) demonstrated the predictive capabilities of natural rubber and chloroprene rubber with different filler concentrations under various types of loading. Bergstrom and Boyce utilized a stochastic micromechanical modeling approach and proposed the reputational movement of the molecules governed the time-dependent behavior of the elastomer. Elastic-plastic behaviors of three-body-centered cubic metal lattices (Khan and Liang 1999) and time-dependent behavior of building materials in general and dynamic (Hann and Sluimer 2001) are effectively addressed by the three-parameter SLS model over a wide range of strain rates and temperatures. Various researchers, as mentioned above, have demonstrated the merits of the SLS model to predict the behavior of elastomers, rubbery materials, bcc metals, and other materials with a time-dependent response. This thesis develops a mathematical constitutive equation using the basic guiding principle behind the SLS model, modifying it to suit the behavior of the capacitive sensor. This report also

discusses its applicability to the SEC as part of WIM systems for its simplicity in inverting the model, effective predicting capabilities, and less computational effort.

4.2 Proposed model structure

A set of experimental data that will be discussed in the next chapter is used to design the rheology model for the SEC. Experimental observations indicated a high degree of nonlinearity in the response along with significant strain-rate dependency in the response for the SEC. The resultant stress-strain responses and the stress histories observed in the above mentioned tests are utilized to identify the physical model parameters. The three-parameter SLS model discussed under section 4.1 is modified for a better understanding of the stress response for the SEC. The modified SLS model with a combination of slider and spring in parallel is demonstrated in Figure 4-4. The equilibrium hysteresis loop is observed under the MSR applied strain history as shown in Figure 5-4. Combining the ideal elastic-to-plastic response of the slider with the nonlinear elastic response of the spring can suitably reproduce this.

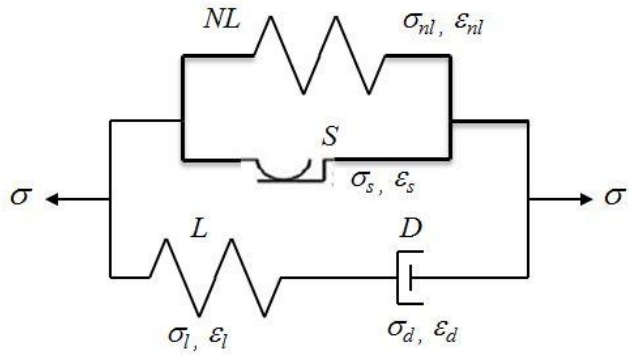

Figure 4-4 : Schematic representation of the constitutive model.

Figure 4-4 demonstrates the stress-strain term representation in the proposed phenomenological model. The branch with spring ‘NL’ and slider ‘S’ together constitutes the equilibrium response of the SEC, while the second branch with spring ‘L’ and dashpot ‘D’ constitutes the rate-dependent response of the SEC.

CHAPTER 5. MECHANICAL BEHAVIOR OF SEC

An experimental scheme is proposed to identify the mechanical behavior of the SEC for the fabricated patches under various rates of loading. UTM-25, a closed loop servo-hydraulic testing machine shown in Figure 5-1 developed by IPC Global, is utilized for this study (Global 2013). The machine contains a 25 kN capacity hydraulically-driven load frame with an environmental chamber to conduct tests over a non-ambient range of temperatures.

Figure 5-1 : Servo-hydraulic testing machine UTM – 25.

The machine is equipped with an Integrated Multi-Axis Control System (IMACS) with internationally accepted test module standards, making it convenient to set up the tests. The environmental chamber is connected with a supply of liquid nitrogen and a heating oven to set the chamber's temperature over a wide range from -40 to +60 deg centigrade. It is also supplied with a feedback system to maintain consistent temperatures during testing. Measurements of axial displacement and axial load applied over the SEC patch

were recorded for all the uniaxial compression tests. Surface dimensions for the SEC patch used during the uniaxial testing are approximately equal to 75 mm x 75 mm. SEC patches of different thickness are used to study the dependence of the resultant stress response on thickness of the patch. Initially, tests were performed with the SEC patch directly under the loading disc without additional set-up and axial displacements are measured by the actuator displacement sensor. The distance moved by the actuator is made equal to the change in the thickness of the SEC. The displacement recordings made by the actuator sensor are deemed inaccurate, considering the thickness of the SEC patch. A new improvised experimental setup with additional plates fabricated using aluminum is proposed as shown in Figure 5-2. Axial displacements in this improvised setup are measured using the Linear Variable Differential Transformers (LVDTs) from IPC Global because of the thinness of the SEC for an improved accuracy in test data. Additionally, fabricated aluminum plates (top and bottom) are used to install the LVDTs for recording axial displacements as shown in the experimental setup. Holes are drilled in the plates for proper alignment to ensure no torsion/bending effects in the LVDT while loading. Accuracy of the Solarton LVDT used for the testing is equal to 0.001 mm and the span of LVDT is equal to 1 mm. The conducted tests are displacement controlled along the vertical axis of the SEC and load cell measured the corresponding force.

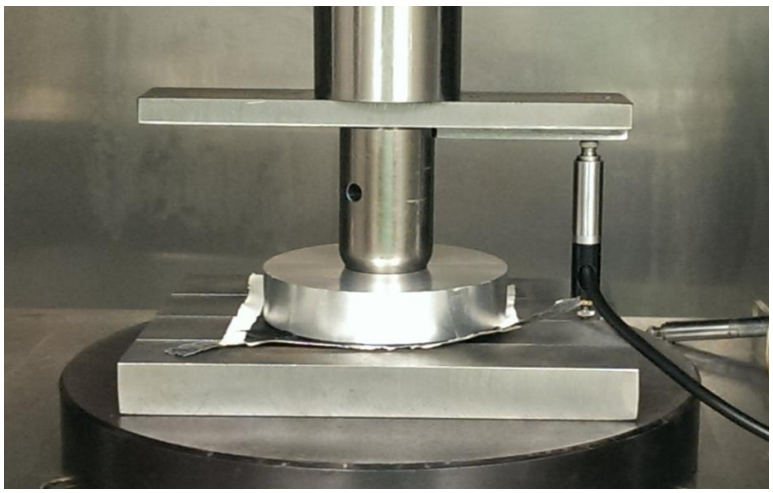

Figure 5-2 : Schematic of the experimental test set up.

An experimental scheme is proposed to identify the set of parameters in the rheological model. Three sets of experiments are performed. They are classified as Multi Step Relaxation (MSR) tests, Simple Relaxation (SR) tests, and Cyclic Compression (CC) tests in the proposed experimental scheme. MSR tests are performed to simulate the equilibrium response (at infinitely slow loading rate) and evaluate equilibrium parameters. SR tests are completed to characterize the viscosity parameters of the rheological model, and the loading path of the SR tests is utilized to simulate the instantaneous response (at infinitely fast loading rate) and identify the instantaneous response parameters. CC tests are achieved to validate the simulated model results against the experimental observations. When the loading rate is very slow, the dashpot element is not virtually active because no force is transmitted through it whereas when the loading rate is high, the dashpot element is blocked as it does not have sufficient time to respond. Therefore, the responses obtained in these tests can be idealized as the viscoelastic response. All data obtained during these tests were recorded using UTS software provided by the IPC Global with real time graph monitoring capabilities. The experimental procedure adopted for this study is similar to the procedure followed by Bhuyian et.al to develop a rheology model of high damping rubbers in compression (2009).

5.1 Span of Loading

The objective of this thesis is to develop a constitutive model for the SEC to employ as part of a WIM system. All specimens are tested under compression with an average absolute maximum compressive stress of 1.5 MPa. This mode of deformations can be considered as more relevant to the WIM system application under the bridge/pavement. Testing and development of the model is given great attention to detail in the stress regime of 0 to 1.5 MPa, considering the fact the SEC-based WIM will be installed under asphalt pavements. A detailed experimental study conducted by Groenendijk et al. (1997) suggests the maximum tire pressure on asphalt pavement does not exceed the limit of 1.5 MPa, considered for testing the mechanical behavior of the SEC. Groenendijk et al. determined the effects of 15 different wheel load configurations, using the linear tracking device (LINTRACK) accelerated loading facility on two pavements: (1) virgin and (2)

loaded with 4 million 75 kN wheel loads. The average contact stress differs from the tire pressure due to the fact that contact pressure is not uniform. Groenendijk et al. demonstrated the super single tire load of 100 kN produced a tire pressure of 1.1 MPa, which develops an equivalent stress of 1.29 MPa. The accumulation of strains over the longitudinal and transverse directions are studied and plotted. The gross weights, as documented by states Department of Transportation for Iowa, Caltrans, Nebraska, and Ohio, shall not exceed 10,000 pounds (45 kN) for maximum single wheel load and 34,000 pounds (152 kN) for maximum tandem axle load. These loads are less than the investigated vehicles in the above tests performed using LINTRACK.

Kim, Bell, and Wilson (1989) conducted a thorough investigation of increased truck tire pressure on asphalt concrete pavements. They also investigated the effect of stress varying over the depth of the pavement and plotted results for different types of tire configurations. Zhong and Otto (1995) worked on the distribution of tire pressure response on asphalt concrete pavements. They plotted a 3D map of the contact stress over pavement, varying with longitudinal and transverse dispersions. Murali Krishnan and Rajagopal (2004) investigated the creep behavior of asphalt concrete under displacement control loading conditions at varying strain rates. They observed as shown in their graphs that the maximum peak stress during the stress strain diagram stays under 1.5 MPa. The same can also be verified by the investigation conducted by Siddharthan et al. (2002)who evaluated pavement response characteristics using finite layer analytical models under varying conditions. The loading conditions reported include two types of tires—conventional and wide base—with different contact stresses. The tire contact stress distributions were studied at different speeds and also for various tire types. The results of all these studies proves the span of load selected for evaluating the model can be deemed as sufficient for application in WIM systems.

5.2 Preloading and Mullins Effect

Elastomeric polymers, rubber-like materials, and glassy polymers exhibit a significant change in their mechanical properties, resulting from the first stretching/compression. This property, exhibited by the virgin materials, was observed by Mullins (1969) and is referred to as the "Mullins effect." Due to the complexity in mechanical response of polymers like the Mullins effect, strain rate dependence, nonlinear behavior, etc., many models were proposed. The mechanical quantity that characterizes the Mullins effect has not been defined, yet. Although this effect has been studied over the past six to seven decades, it still poses challenges in terms of modeling and physical understanding. The first cycle of stress-strain curve differs significantly from the subsequent cycles because of this effect. Diani, Fayolle, and Gilormini (2008) have completed a detailed review on the Mullins effect; work achieved on this topic over the past six decades, and presented experimental evidence along with various proposed theories. These theories favored the emergence of laws of mechanical behavior.

To limit the impact of the Mullins effect on the polymer response, the polymers are preloaded to a certain extent before beginning the actual tests. Harwood, Mullins, and Payne (1965) observed the polymer response becomes repeatable after the first few stages of loading. The specimens for testing were preloaded for 5 to 6 cycles, gradually increasing amplitude to a final peak strain to overcome the Mullins effect. The virgin SEC patches were subjected to preloading to remove the Mullins effect and softening behavior. SEC patches were treated with 10 cycles of cyclic loading at a strain rate of 0.025 mm/s to a stress level of 3.5 MPa to obtain a stable mechanical behavior. The preloading was repeated 2-3 times until a repeatable stress-strain response was observed. The preloading was repeated before the start of MSR and SR tests, as a precautionary measure to avoid softening. A time gap of 2-3 min was allowed to keep the healing effect of the material constant for all tests (Bueche 1961).

5.3 Multi-step Relaxation Tests (MSR tests)

The equilibrium response for the polymer material at an infinitely slow loading rate is described in Figure 4-2. It is not practically possible to attain an infinitely slow rate of loading, due to the inherent viscosity property and due to the physical constraints with the loading apparatus; hence, the MSR tests were performed to simulate an infinitely slow rate to identify the equilibrium response parameters in the rheological model. Amin et al. (2002) employed similar kinds of tests to develop a mechanical model of the rubber-like polymers. The strain history data presented in Figure 5-3 show multiple periods of relaxation for a time duration of two and one-half minutes, when the applied compressive strain is held constant, and inserted into the path of loading and unloading the SEC. Figure 5-4 shows the resultant equilibrium stress response and the equilibrium hysteresis observed under this applied loading. The test is repeated with varying rates of loading.

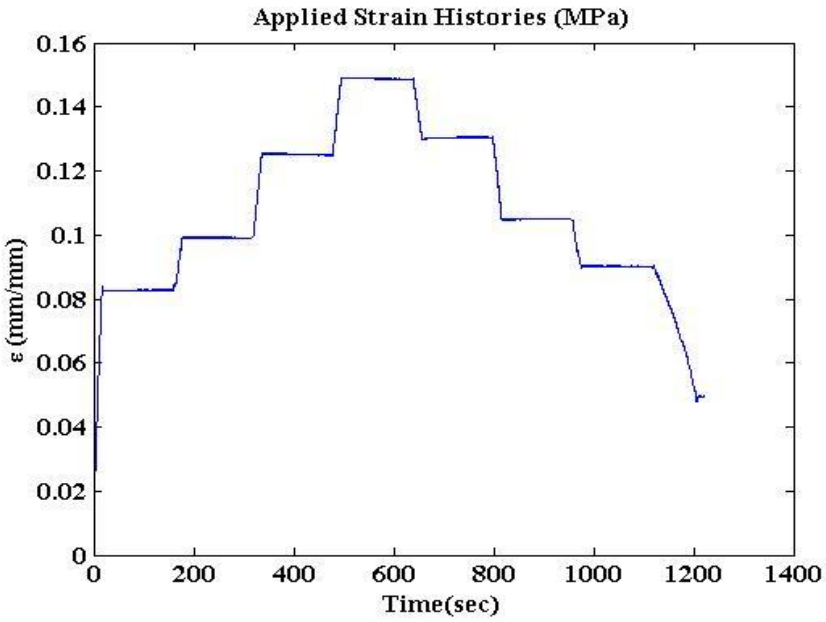

Figure 5-3 : Applied strain histories in a MSR test on a flexible patch; a compressive strain rate of 0.0075 mm/s is held constant at each strain step.

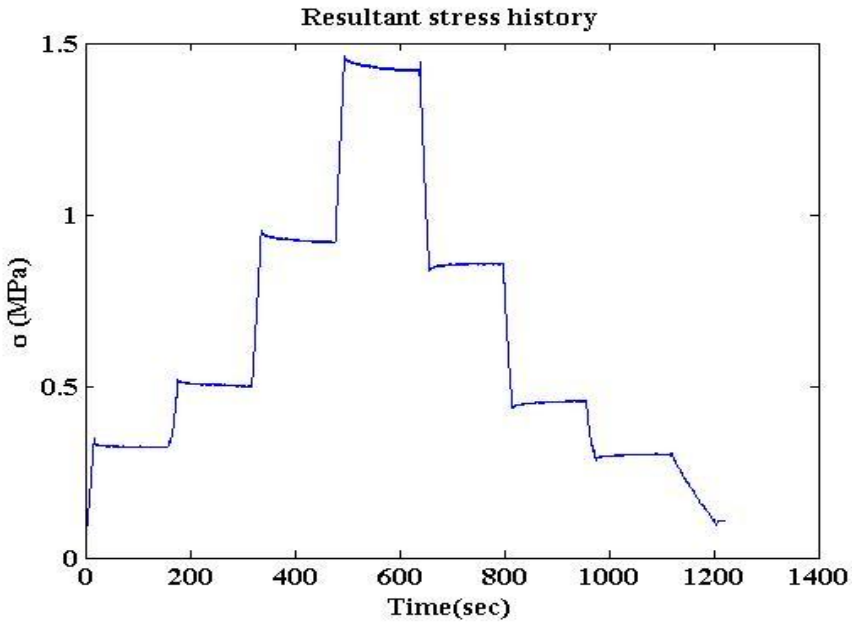

a)

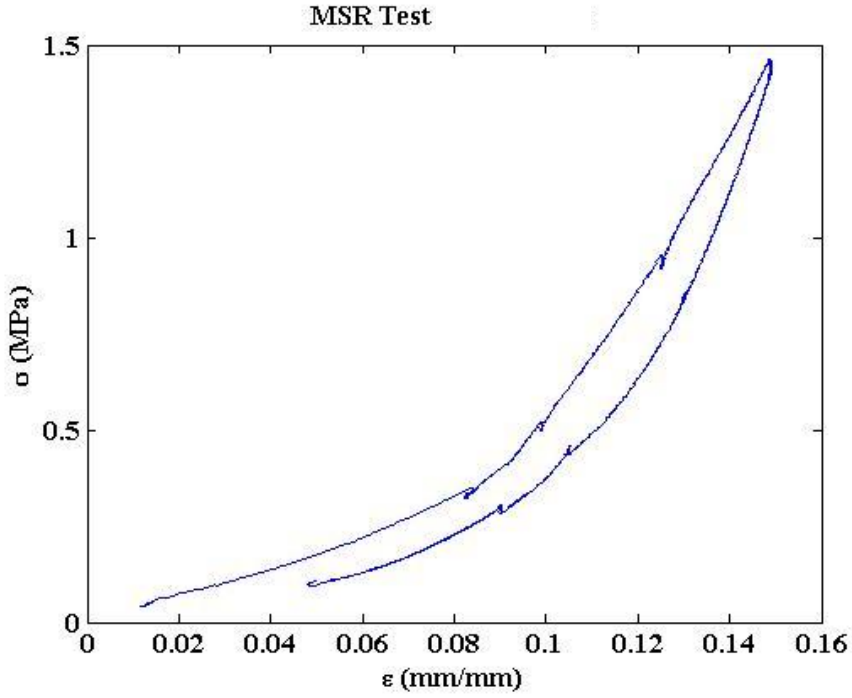

b)

Figure 5-4 : Typical MSR test results a) stress history b) equilibrium strain-strain response.

5.4 Simple Relaxation Tests (SR tests)

The MSR tests mentioned in section 5.3 are used to simulate and evaluate the equilibrium parameters. Therefore, the remaining parameters of the model for evaluation are the instantaneous parameters to define the immediate response of the SEC and viscosity parameters to define the viscous response of the SEC. A series of SR tests are performed by compressing the SEC to various strain levels, as shown in Figure 5-5. The observed stress histories shown in Figure 5-6 illustrate the rapid stress relaxation displayed in the initial few minutes. After a while, it appears to have converged to a constant state of stress similar to what is observed in the MSR tests. The converged state of response can be regarded as the equilibrium state of response. This can be attributed to the chemical composition of the SEBS and the molecular chain network of the SEBS. In the initial stages of the SR test, a sudden strain occurs more rapidly than the accumulation capacity. But, as time elapses, the molecular chains unwind and only a less amount of stress is needed to maintain the constant strain level in the SEC. The amount of stress relaxation observed in the loading path differs from the stress relaxation observed in the unloading path.

Relaxation behavior of the SEC is independent of the amount of stress in the model. This can be observed by comparing the resultant stress histories in Figure 5-6. Although the amount of stress is different with the rate of loading, the relaxation almost looks the same, thus, proving the point. Relaxation behavior is also observed to be independent of the rate of loading. It can be seen from the applied strain histories that different rates of loading are applied to reach the strain level. Independent of the strain rate applied and the level of strain, the relaxation followed a similar path to converge to the equilibrium state. Because the thickness of patch is small, the amount of stress relaxed to reach the state of equilibrium cannot be observed in Figure 5-6.

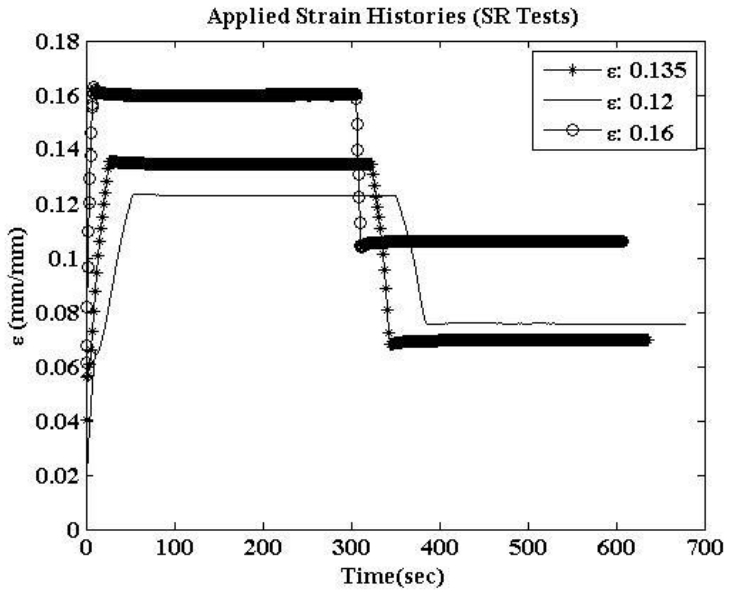

Figure 5-5 : Strain histories applied in simple relaxation tests on thin patch; compressive strain rate is held constant for each time step.

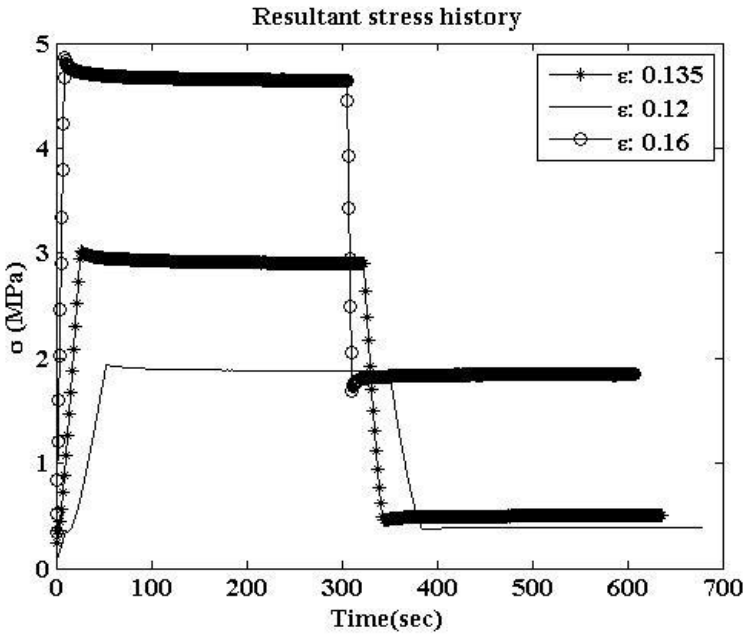

Figure 5-6 : Typical compressive stress histories observed in simple relaxation tests.

An instantaneous response demonstrated in Figure 4-2 is observed under infinitely fast rate of loading. But, it is practically unfeasible to attain the infinite rate as the displacement controlled servo-hydraulic machine has an upper bound on the rate of strokes. The loading path for SR tests can be used to estimate the instantaneous response of the SEC patches. Rate-dependent compressive stress-strain responses are observed as seen in the resultant stress. The constant strain rate is maintained until the maximum strain level is attained. . Stress-strain histories over a wide range of loading rates mark an interesting observation about the rate-dependent response. A stronger rate dependency is seen in the loading phase against the weaker rate-dependent stress-strain response in the unloading phase. A diminishing trend for stress responses is observed at the higher strain rates, indicating the neighborhood of the instantaneous state of response.

5.5 Cyclic Compression Tests (CC tests)

Four cycles of loading and unloading are applied at various strain rates. Three are shown in Figure 5-7. A constant strain rate was maintained for each cyclic test within a range of 0.0005 to 0.2 mm/s until an average maximum strain level of 0.12 mm/mm is attained. Figure 5-8 presents the stress-strain response as obtained from the cyclic compression tests under three different rates of loading. Six tests were conducted with different strain rates in cyclic compression. A sloping trend of responses is observed with increasing strain rates. The strain rate dependence of the SEC is demonstrated in Figure 5-8. It can be seen the stress response increased with the increase of strain rates. The presence of hysteresis is visible in the observed stress-strain responses. The stress responses observed in Figure 5-8 appeared nonlinear at all strain levels. The permanent set behavior is determined much lower in the SEC in comparison to most of the available polymers. A small amount of acceleration is observed in the strain data, due to a jerk in the hydraulics of the machine at relatively the same strain level in all the tests. Cyclic compression test results are used to validate the proposed model for investigating the efficiency of the proposed experimental scheme and the constitutively developed physical model.

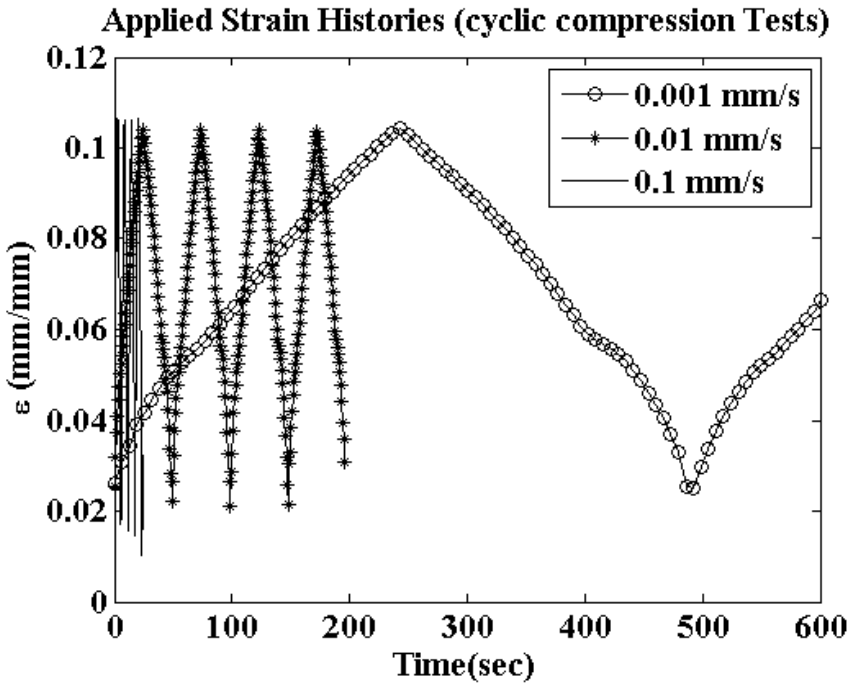

Figure 5-7 : Strain histories applied in cyclic compression tests.

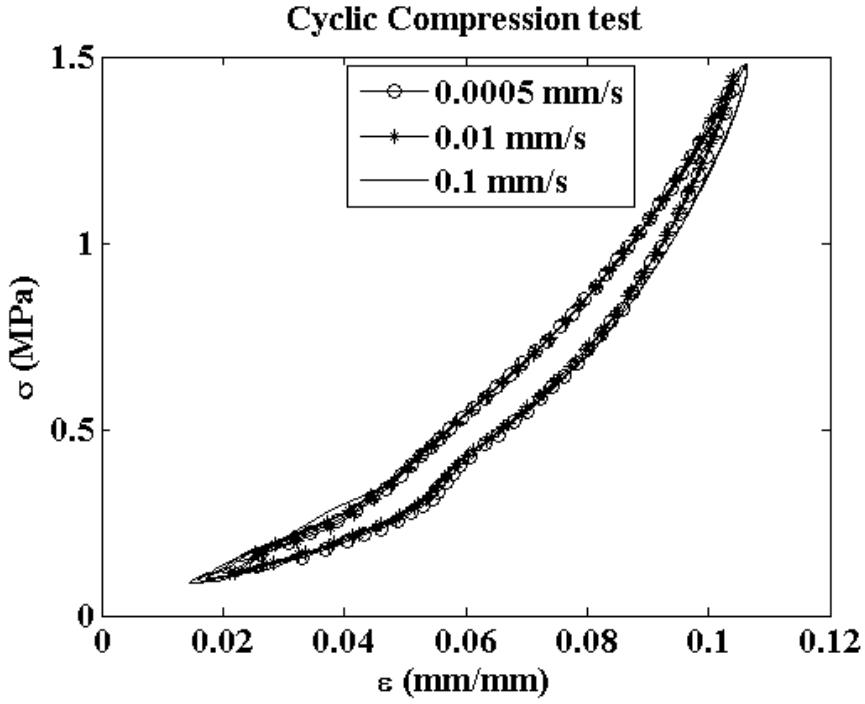

Figure 5-8 : Typical stress-strain responses obtained from cyclic tests.

5.6 Parameter evaluation approach

The experimental scheme performed is used as pictorially described in Figure 5-9 to identify and evaluate the parameters of the spring and dashpot elements. Equilibrium hysteresis, the fundamental part of the response of the SEC obtained from the MSR test data, is used to identify the equilibrium spring parameters. Nonlinear spring elements are required to represent the observed nonlinear equilibrium response, in contrast to a linear viscoelastic model. When the rate of loading is very slow, i.e., when the velocity of strain is equal to 'zero' dashpot, element D is not virtually active, since it does not transmit any force through it. As a result, the model's response is constructed using spring element, NL, and slider, S. Therefore, the MSR test data are used to identify the parameters of the spring and slider in the first branch. When the rate of loading is very high in the neighborhood of the instantaneous state, i.e., when the velocity of strain is very high, due to the insufficient amount of time to deform the dashpot, element D is blocked. As a result, both the spring elements, NL and L, and slider, S, constitute the response for the model. Therefore, the loading path of the SR test data is used to identify the parameters of the spring in the second branch (spring in the Maxwell element). Finally, the viscosity parameters of the dashpot, D, are identified, using cyclic compression data based on the nonlinear optimization techniques.

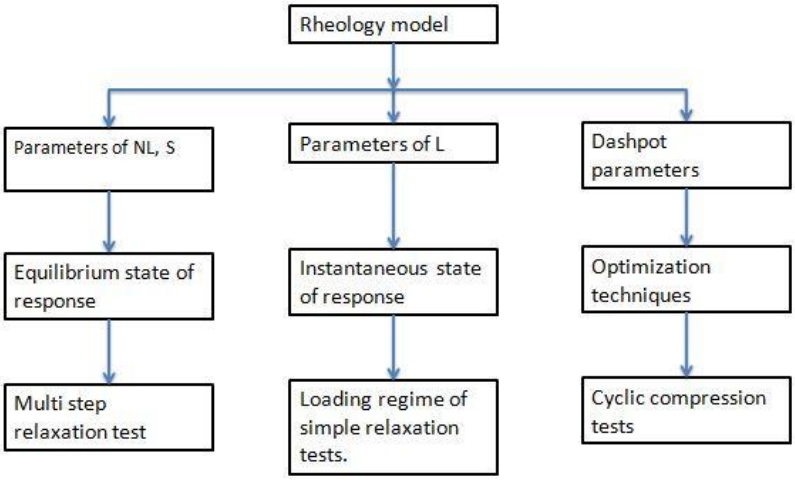

Figure 5-9 : Flow chart demonstrating the parameter identification of the rheology model.

CHAPTER 6. RHEOLOGY MODEL

The mechanical behavior of SEC comprises both rate-dependent and rate-independent responses. These responses motivate design of the basic structures of the viscoelastic rheology model as shown in Figure 5-9. In this model, the total stress (σ) is decomposed into two parts equilibrium stress (σ_{eq}) and overstress (σ_{os}) (see Figure 4-3). Equilibrium stress is the stress in the branch with a spring and slider, while the overstress is the stress in the second branch with spring and dashpot (also called Maxwell element). In addition to the stress, strain in these elements can also be decomposed as shown in Eq (6-2).

$$\sigma = \sigma_{eq} + \sigma_{os} \,. \tag{6-1}$$

$$\varepsilon = \varepsilon_{nl} = \varepsilon_s = \varepsilon_l + \varepsilon_d \,. \tag{6-2}$$

In the subsequent sections parameter identification scheme for rate independent part of the constitutive model is discussed followed by the rate dependent part of the model.

6.1 Equilibrium Response

From a typical MSR stress response, equilibrium hysteresis loop is observed in the behavior of the SEC patch. According to the standard SLS/Zener model described in the Chapter 3, the equilibrium response is constructed by the spring element parallel to the Maxwell element. However, to model the observed hysteresis, a slider with a sigmoid mathematical relation between the stress and strain has been adopted in the proposed model. To a large extent, stress responses of the MSR tests appear to be nonlinear elastic, similar to a Newtonian spring. Hence, the slider is mainly incorporated to model the observed equilibrium hysteresis. The sigmoid function offers the privilege of a smooth transition from loading to unloading (positive velocity to negative velocity) that result in hysteresis. The sigmoid function has been chosen because response of the slider is assumed to approach a saturated value, as the time elapses, and the nonlinear spring

constitutes the remainder of the equilibrium response thereafter. Interaction between the stress and strain of the slider is modeled in Eq. (6-3).

$$\sigma_s = {f1}\Big/{(1 + e^{-100\times(\epsilon - f2)})} \times sgn(\dot{\epsilon}) \ , \qquad (6\text{-}3)$$

where f1, f2 are the constants for slider S with sgn($\dot{\epsilon}$) = +1 if $\dot{\epsilon} > 0$ indicates the loading regime; -1 if $\dot{\epsilon} < 0$ indicates the unloading regime.

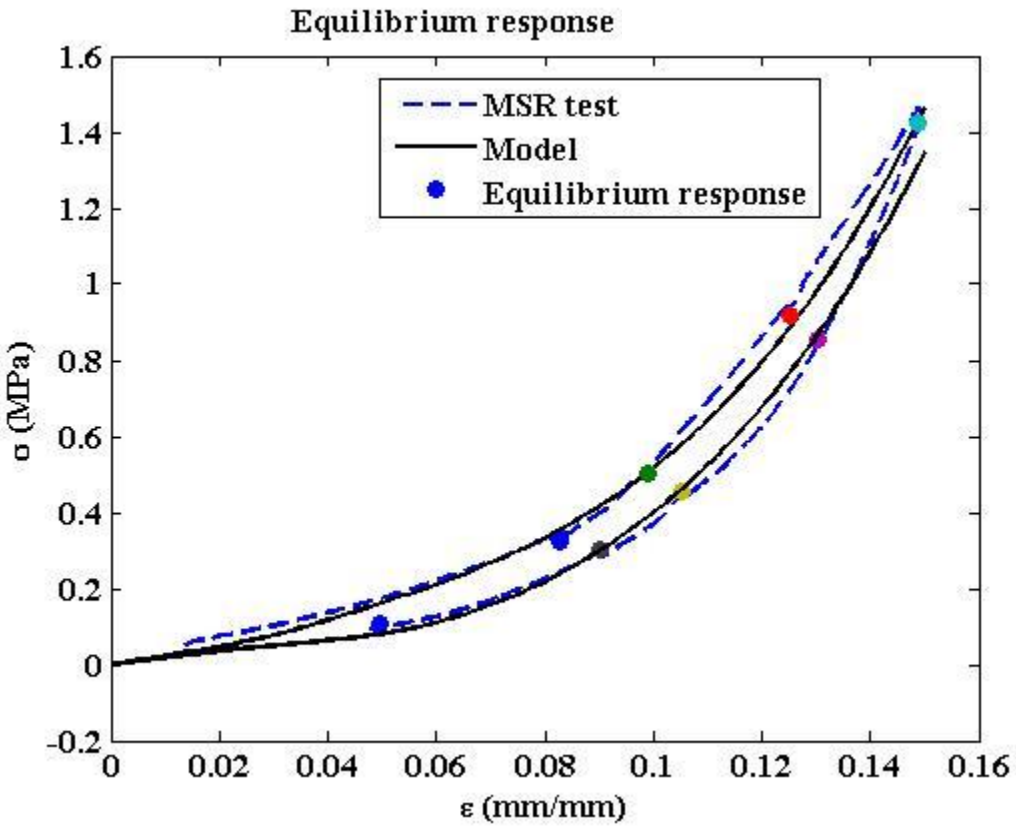

Figure 6-1 : Identification of parameters – Equilibrium response.

To express the nonlinear behavior of the observed stress response in the MSR tests, a nonlinear spring is utilized for the element 'NL'. An exponential resultant stress-strain behavior is observed from the experimental recorded data under multi step relaxation tests. Therefore a nonlinear exponential equation is assumed to model the stress and strain relationship in the spring 'NL'.

$$\sigma_{nl} = c1 \times \in + c2 \times \in^{c3}, \quad (6\text{-}4)$$

$$\sigma_{eq} = \sigma_s + \sigma_{nl}. \quad (6\text{-}5)$$

The parameters for rate independent equilibrium response are determined, using the recorded MSR test data under various rates of loading. Parameter f1 is selected, using the equilibrium hysteresis loop, such that it approximately corresponds to the average difference between the loading and unloading stresses at each strain level. Next, parameter f2 is selected, such that the sigmoid reaches its peak value, f1, from the strain level at which the stress-strain response starts to become significantly nonlinear. Finally, the parameters for the nonlinear spring must be identified to construct the equilibrium response completely. Subtracting the stress, $\sigma_{s,}$ from the equilibrium stress obtained in the MSR test results provides the stress corresponding to the stress in the nonlinear spring, σ_{nl}. By using the standard unconstrained least squares optimization technique, the parameters—c1, c2 and c3—are determined. A similar procedure is repeated for both stiffer and flexible patches. The obtained parameters for the spring and slider for both patches are tabulated in Table 6-1. Evaluated parameters are utilized for simulating the equilibrium response, using the proposed model and the experimental results are presented in Figure 6-1. A dotted line in Figure 6-1 indicates the resultant stress response, while the scatter points indicate the trend of convergence to a relaxation state at the end of each relaxation period. These scatter points collectively represent the equilibrium response of the SEC patch.

Table 6-1 : Elastic response parameters of the SEC patches

Type of patch	C1	C2	C3	F1	F2	D
Stiff	5.3937	1016.9	3.2644	0.059	0.042	0.3934
Flexible	2.0062	1012.4	3.5960	0.059	0.042	0.5053

6.2 Instantaneous Response

For this instance, the constitutive model can be reduced to the similar model without the dashpot element. Owing to the infinitely high strain rate of loading, the dashpot element is fixed and, consequently, the response of the model can be evaluated by adding the overstress to the existing evaluated model. In the neighborhood of the instantaneous response, overstress can be assumed the contribution from the spring element 'L' without the dashpot element 'D'. The loading regime of the SR tests is utilized to evaluate the spring parameters. From the SR test results, a diminishing trend in stress response is observed with increased loading rates. Hence, maximum strain rate in the current SR tests is assumed in the neighborhood of the instantaneous response. Similar to the equilibrium response, the instantaneous response appears nonlinear at each strain level. However, for computational simplicity and for ease to invert the model in WIM system applications, a linear spring constant is employed for the spring element 'L'.

$$\sigma_{oe} = D \times \varepsilon_l \,. \qquad (6\text{-}6)$$

Because the dashpot is assumed fixed for the instantaneous response, strain in the spring element 'L' is equal to the strain in the SEC patch, based on Eq. (6-2). Overstress, σ_{oe}, can be evaluated by subtracting the equilibrium stress due to the slider and nonlinear spring from the stress response observed in the loading regime of the SR tests. Parameter D is evaluated such that the sum of overstress and equilibrium stress can envelop the stress-strain curves in the loading regime obtained for SR tests. Figure 6-2 shows the comparison between the simulated model and the instantaneous stress-strain curve, and also represents the equilibrium response. A similar procedure is adopted for the flexible patch and the evaluated parameters are tabulated under Table 6-1.

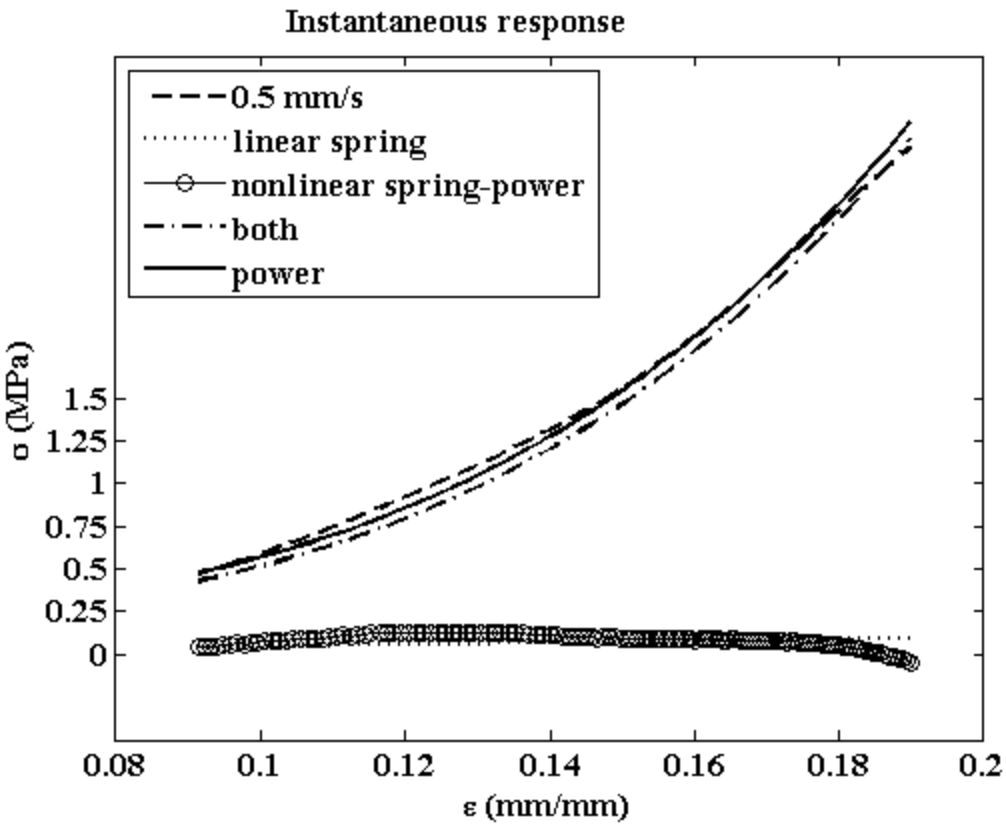

Figure 6-2 : Identification of parameters – Instantaneous response.

6.3 Viscosity Parameters

Since we identified the elastic parameters of the proposed model, we are left with identification of the viscosity parameters of the dashpot element, 'D'. The relaxation data obtained from the SR tests are analyzed to evaluate the dashpot parameter. This section details the procedure to procure a mathematical relationship between overstress, σ_{oe}, and the dashpot strain rate, '$\dot{\varepsilon}$d. Assuming the resultant stress response at the end of each relaxation is the equilibrium response at a particular strain level, overstress is estimated in a similar procedure described in section 6.2 by subtracting the equilibrium stress from the total stress response. Time history of the strain in the spring 'L' within the Maxwell element is computed using the Eq. (6-5). Summation of the strains in the dashpot and spring components is equal to strain in the spring element, NL, equal to the applied strain

as mentioned in Eq. (6-2). Therefore, time history of the dashpot strain is computed by subtracting the strain in the spring element ‘L’ from the total strain.

Owing to the small thickness of the SEC test specimen, there is a considerable amount of scattering in the strain data, due to noise. The noise might be due to various possible reasons like the magnitude of the UTM testing machine used for testing thicker asphalt specimens and the movement of the actuator dependent upon the hydraulics. Therefore, a moving average technique was adopted before taking the time derivative of the computed time history of the dashpot strain using a five-point stencil differential method. Nonlinear relationship is observed between the dashpot strain rate and the overstress. Also, it is seen the relationship nearly follows a power law and the equation described in Eq. (6-7) is used to model the dashpot.

$$\sigma_{oe} = K1|\dot{\varepsilon}d|^{K2}, \qquad (6\text{-}7)$$

where K1 and K2 are the viscosity constants.

The figurative plot is constructed, using the stress relaxation data in loading. However, the author decided these data cannot be used to identify the constitutive relationship of the dashpot due to following reasons.

- Due to the limitation with dimensions of the SEC test specimen, the strain relaxation is found to be significantly low. This has impacted the computed dashpot strain rate. A rapid amount of stress relaxation occurs in the first few minutes, when the strain is held constant and the highest velocity observed during this time frame is close to 0.002 /sec. This is not sufficiently high to develop a physical relationship between the dashpot strain rate and overstress.
- The amount of stress relaxed when the strain is held constant is less than five percent of the maximum stress obtained during the SR test. It can be seen in Figure 6-1 that the difference in stress during loading and unloading at a

particular strain level is more than the observed stress relaxation over the entire span of loading.

- The servo hydraulic testing machine is not able to attain the zero strain rate during simple relaxation tests. Strain data recorded is used to compute the velocity using a five point differential method. It is observed that the computed loading rate fluctuated significantly when the applied strain is held constant.

Owing to these reasons and understanding the behavior of the SEC under various test conditions, the author used an optimization technique to determine the constitutive relationship of the dashpot.

It is noticed the overstress is significantly different in the loading and unloading regimes. Hence, a different dashpot parameter is required for loading and unloading to model the physical relationship of the dashpot. A similar power law relationship has been adopted to model the dashpot as shown in Eq. (6-7). Furthermore, it is found the overstress depends on the strain levels in the relaxation data; therefore, parameter K1 is evaluated, using strain histories of the test data at different strain levels. This parameter varies in loading and unloading, and is evaluated accordingly. An applied strain rate is computed to distinguish between loading and unloading at every instant. The moving average technique has been applied before computing the time derivative of the applied strain history. Therefore, K1 is the parameter to switch viscosity between loading and unloading. As motivated from the observed overstress-dashpot strain rate relationships obtained in the SR tests results, parameter K2 is kept the same in both loading and unloading conditions. The nonlinear viscosity parameters in this mathematical relationship are evaluated, using numerical techniques. The procedure for determining the viscosity parameters, K1 and K2, is discussed next.

Cyclic loading history completed under cyclic compression (CC) tests is used to determine the switching parameter, K1, and the power parameter, K2. K1 is chosen as an adaptive parameter that constantly changes with strain. Cyclic compression test history corresponds to the tests described under section 5.5. An optimization technique, based on

the unconstrained least squares technique, is employed to solve for the parameters. The mathematical description of the optimization problem is defined as minimizing the error function presented in the Eq. (6-8)

$$\text{Minimize error} = \sum_1^N (\sigma exp, n - \sigma model, n)^2 \ . \qquad (6\text{-}8)$$

N stands for the length of the available strain history data or the data points of interest and $\sigma_{exp,n}$ corresponds to compressive stress response at any instant obtained from the experiment, while $\sigma_{model,n}$ corresponds to the simulated stress at any instant, using the proposed model. Using a standard approach available in Matlab, the optimization problem is solved to minimize the error function. The corresponding values for K1 (range over which K1 value changes because K1 is adaptive to strain) and K2 for both the stiff and flexible patches are presented in Table 6-2.

Table 6-2 : Viscosity parameters of the SEC patches

Type of patch	K1	K2
Stiff	0.0475-0.4091	0.0699
Flexible	0.0267-0.1857	0.2862

Experimental observations presented in Chapter 5 revealed the rate dependent behavior, along with viscosity, induced properties for the SEC patches. Utilizing the experimental test data observations, nonlinear and linear spring parameters, parameters for slider to switch between loading and unloading in the equilibrium response, and viscosity parameters are evaluated as described in previous sections. Numerical simulations of the loading data are presented in Chapter 7. Differences in the resultant stress response of the stiffer and flexible patches are discussed and interpreted, using the evaluated parameters.

CHAPTER 7. NUMERICAL SIMULATIONS AND DISCUSSIONS

7.1 Deriving the Stress Equation

Now, we have evaluated all parameters using the proposed experimental scheme. The stress response is simulated under various test conditions and compared against the obtained experimental data. The equation to model the stress response is derived using the equations mentioned in Chapter 6.

The proposed model has a Maxwell element in parallel to a combination of spring and slider. Utilizing the equations proposed in Chapter 6, interrelations between the stress and strain variables of these elements are evaluated, as given in Eq. (7-1).

$$\sigma = \sigma_m + \sigma_{nl} + \sigma_s \,;\, \sigma_m = \sigma_l = \sigma_d \,. \tag{7-1}$$

$$\varepsilon = \varepsilon_m = \varepsilon_{nl} = \varepsilon_s;\, \varepsilon_m = \varepsilon_d + \varepsilon_l.$$

Where, subscripts m, s, nl, l, and d stand for Maxwell element, slider, nonlinear spring, linear spring, and dashpot, respectively. Based on the relationships described above and Eq. (6-7) ,we can rewrite the dashpot strain rate in terms of resultant stress, σ, and stress in the nonlinear spring, $\sigma_{nl.}$

$$\sigma_d = \sigma - \sigma_{nl} - \sigma_s \,. \tag{7-2}$$

$$\mathrm{sgn}(\dot{\varepsilon_d}) = \left(\frac{(\sigma - \sigma_{nl} - \sigma_s)}{K1}\right)^{1/K2} \,.$$

Because there is an absolute sign included in the mathematical relation of the dashpot parameters, interchanging the terms resulted in a sign function. We can also rewrite the interdependence of stress in the linear spring element with stress in the nonlinear spring element,

$$\sigma_l = \sigma - \sigma_{nl} - \sigma_s . \quad (7\text{-}3)$$

Taking a time derivative of Eq. (7-3) and interchanging the terms to subject, ε_l ,will give an equation in terms of evaluated parameters and stress components in other elements.

$$\sigma_l = \sigma - \sigma_{nl} - \sigma_s . \quad (7\text{-}4)$$

$$\dot{\varepsilon}_l = (\dot{\sigma} - \dot{\sigma}_{nl} - \dot{\sigma}_s)/_D .$$

Using Eqs. (7-1, 7-2) and (7-4), we can combine all equations into one single term,

$$\dot{\varepsilon} = \dot{\varepsilon_d} + \dot{\varepsilon_l} \quad (7\text{-}5)$$

$$\dot{\varepsilon} = \left(\frac{(\sigma - \sigma_{nl} - \sigma_s)}{K1}\right)^{1/K2} + \frac{(\dot{\sigma} - \dot{\sigma_{nl}} - \dot{\sigma}_s)}{D}.$$

Because the slider approaches its saturate peak stress value at considerably low levels of strain as explained in section 0, the time derivative of the slider stress response is approximated as equal to zero. Rearranging the terms in the above equation, the time derivative of the simulated stress response can be written as

$$\dot{\sigma} = (D + \dot{\sigma_{nl}})\,\dot{\epsilon} + D * sgn\left(\frac{(\sigma_{nl} + \sigma_s * \mathrm{sgn}(\dot{\epsilon}) - \sigma)}{K1}\right) * \left(\left|\frac{(\sigma_{nl} + \sigma_s - \sigma)}{K1}\right|\right)^{1/K2} \quad (7\text{-}6)$$

where the equations for the stress in the nonlinear spring element, ‘NL’ , linear spring element, ‘L’ , slider, ‘S’, and dashpot, ‘D’, are same as explained in Chapter 6. Therefore, they can be substituted accordingly to evaluate the stress computed by the model. A numerical integration technique with a time step equal to the time step in the time history of applied strain data is used with Matlab to solve the mathematical relationship of the stress rate described in Eq. (7-6) for computing the stress at every time step.

7.2 Simulations

7.2.1 Cyclic compression tests

A model based on viscoelastic theory is formulated under section 4.2; along with proposals to evaluate the parameters for minimizing the error between model prediction and experimental observation. In this section, Eq. (7-6) is used to simulate the observed resultant stress response under the applied loading histories (strain data) mentioned in CHAPTER 5. The evaluated elastic and viscosity parameters tabulated under Table 6-1 and Table 6-2 are employed to simulate the cyclic compression tests. Simulations of the MSR and SR tests, as well as their comparison with experiment data, follow.

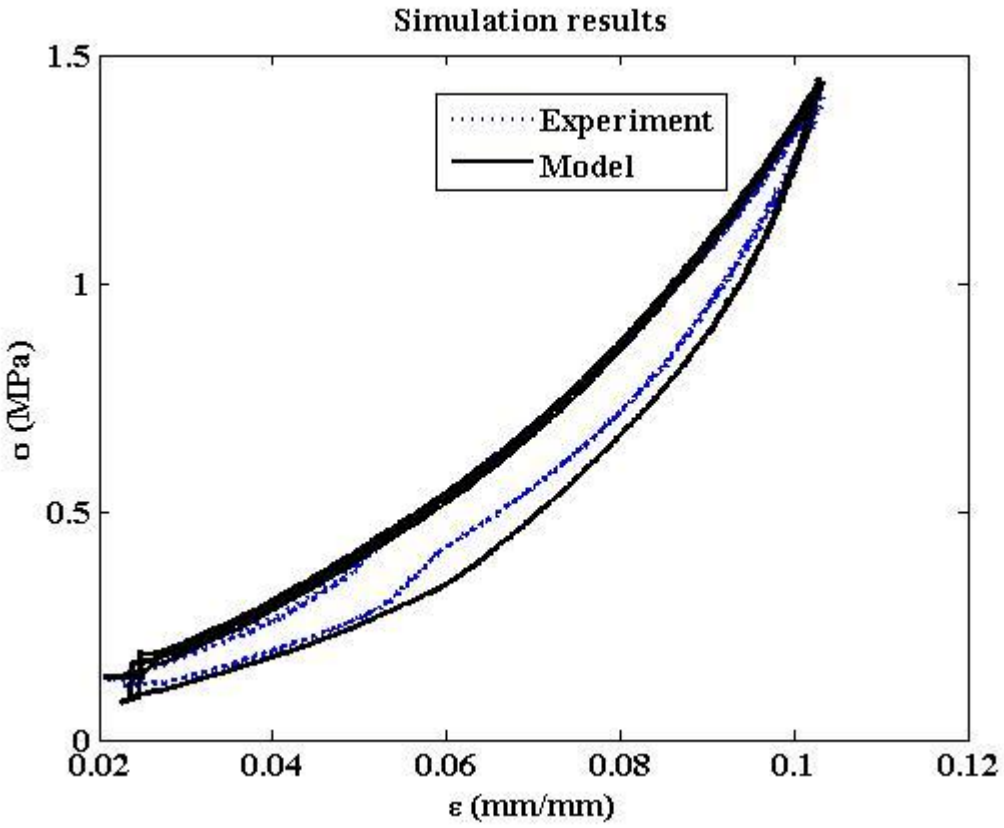

a)

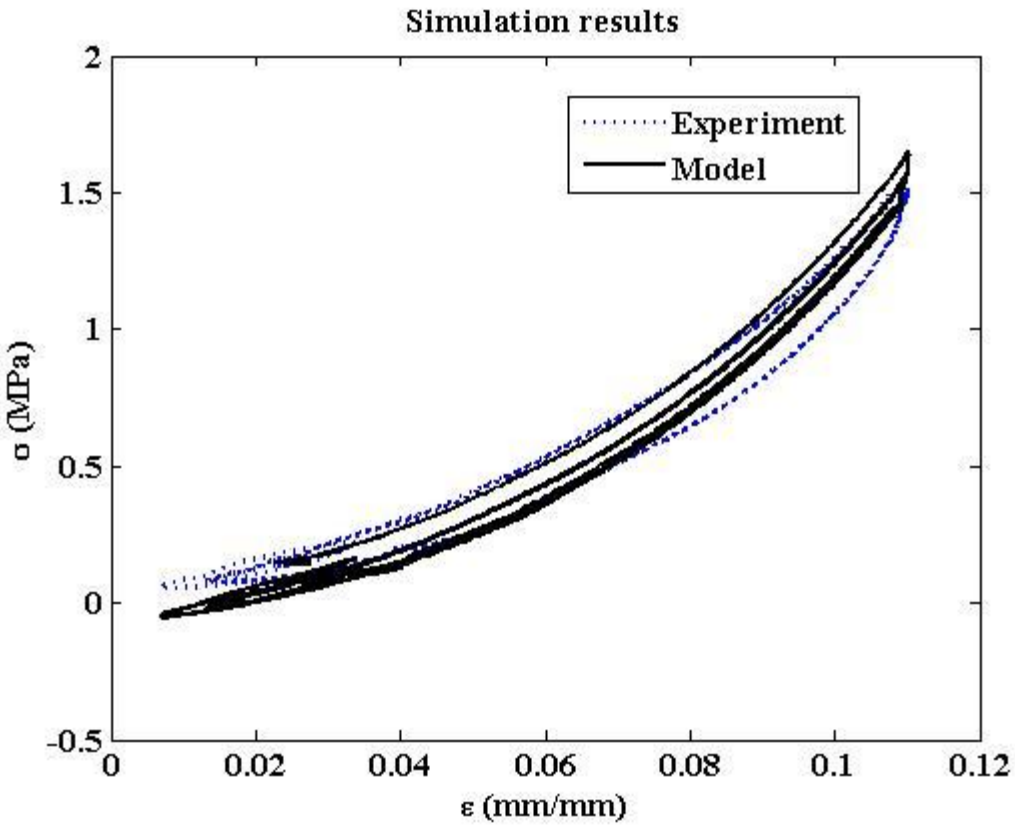

b)

Figure 7-1 : Numerical simulations of cyclic loading data – Stiffer patch a) strain loading rate – 0.0025 mm/s b) strain loading rate - 0.25 mm/s.

The simulated stress response data in cyclic compression loading conditions are compared against the experimental observations at various strain rates. Figure 7-1 shows the comparison at relatively slow and fast rates of loading on the stiffer patch. One can see the simulated model closely matches the experiment data at both of these rates. However, there is a small increase in the absolute maximum error value from 0.084 to 0.135, still sufficient for predicting the loads in WIM system applications. A similar procedure is adopted for flexible patch under cyclic loading conditions. Figure 7-2 shows the simulated data fit well at both slow and faster loading rates. The absolute maximum error has increased from 0.08 to 0.185, as the loading rate increased from 0.005 to 0.15 mm/s.

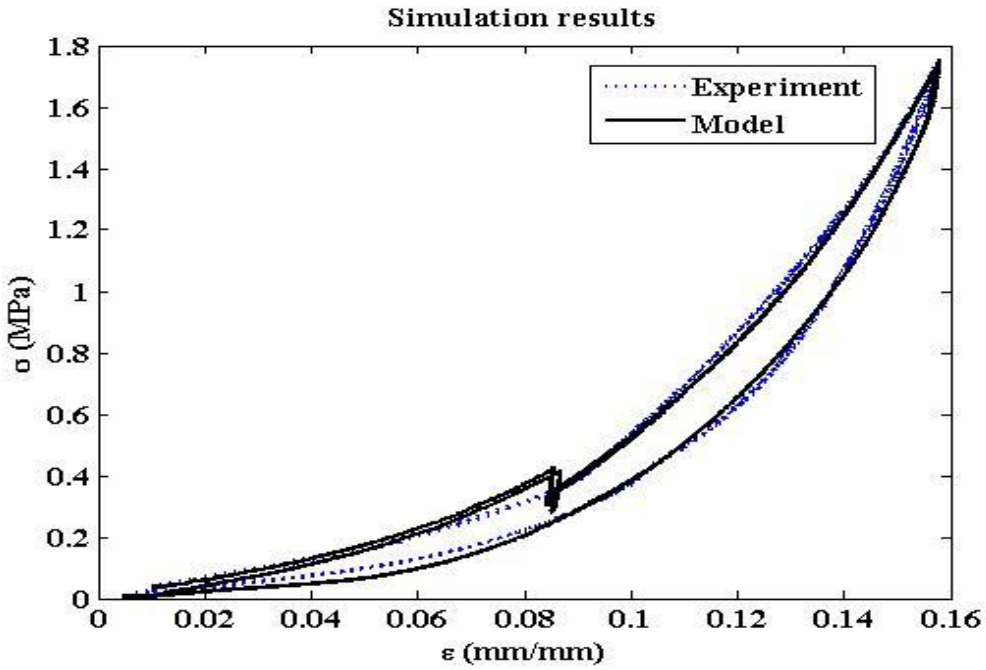

a)

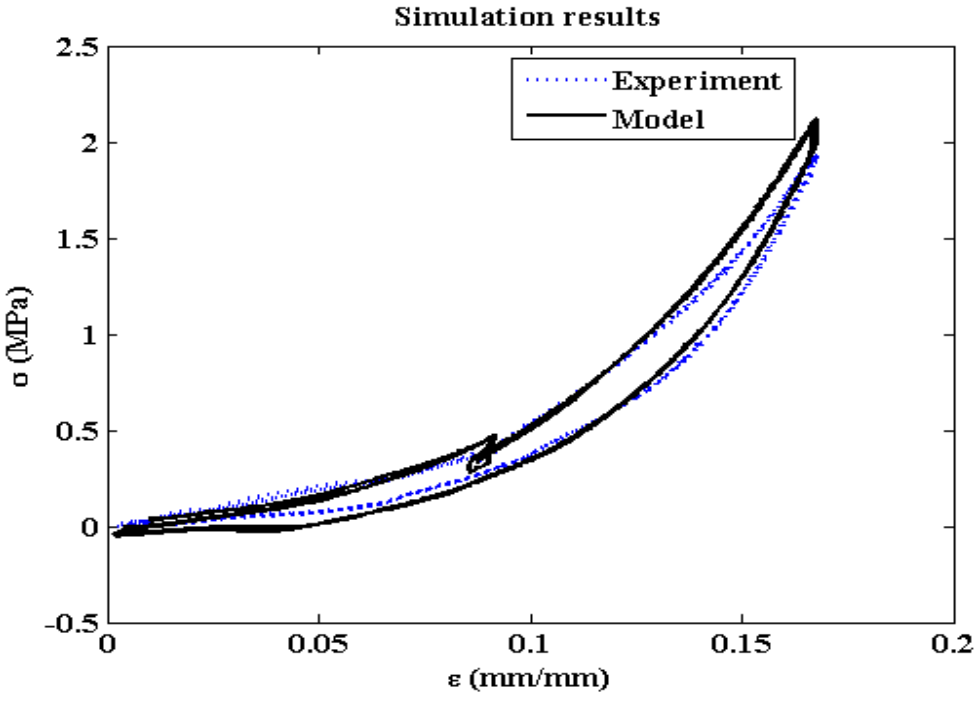

b)

Figure 7-2 : Numerical simulations of cyclic loading data – Flexible patch a) strain loading rate – 0.005 mm/s b) strain loading rate - 0.15 mm/s.

7.2.2 Relaxation tests

We have observed the simulated stress results match closely with the experiments in representing the instantaneous and equilibrium responses that construct the cyclic stress response. However, as shown in the figures above, the agreement between the simulated stress response and the experiment at fast loading rates is not well compared to the slower loading rates. The stress rate equation derived under section 7.1 is used to compare the observed amount of stress relaxation in the experimental data against the modeled response.

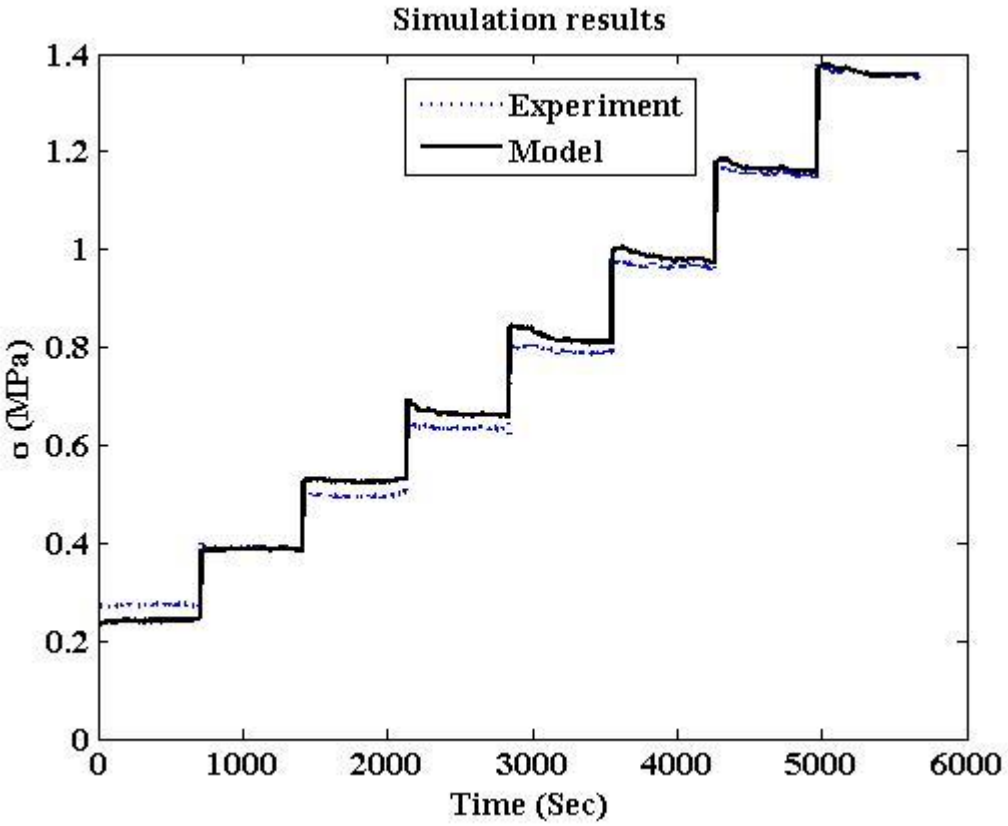

a)

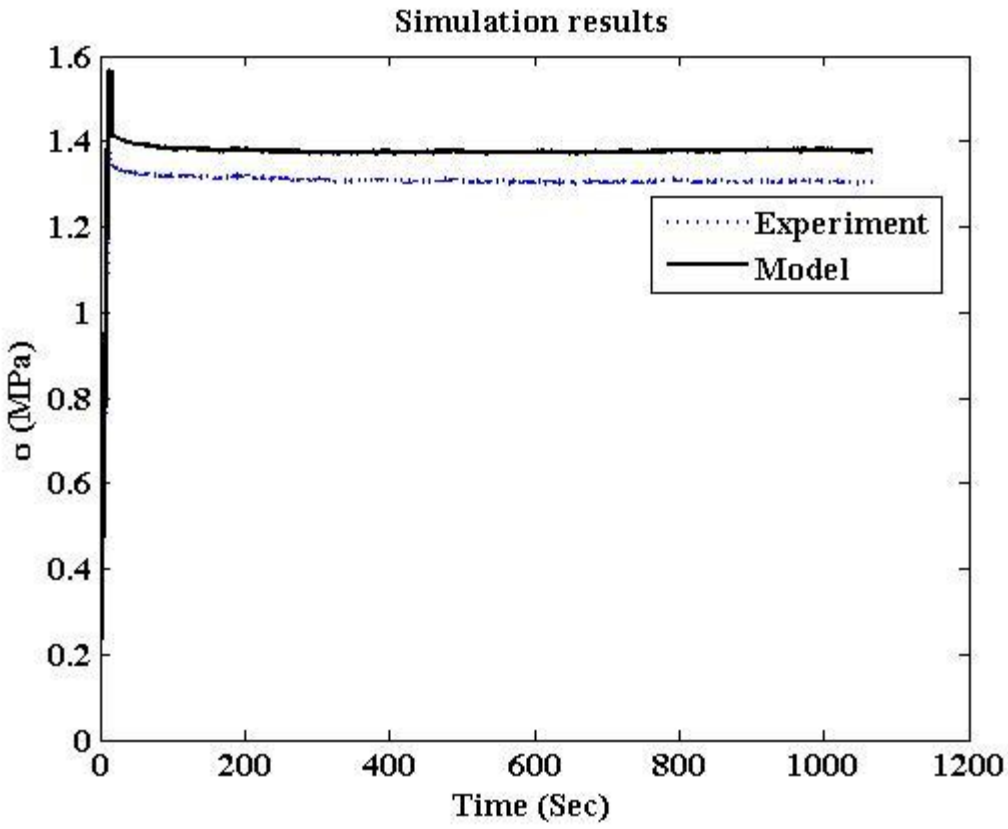

b)

Figure 7-3 : Numerical simulations of relaxation test data a) MSR test b) SR tests

Figure 7-3 shows the experiment obtained MSR data fit well with the simulated data. This can be interpreted from the fact the equilibrium hysteresis is closely matched, using the proposed nonlinear spring and the slider in section 6.1. However, a significant amount of stress is released immediately after the strain is held constant, compared to the experiment data which asymptotically converges to an equilibrium state as observed in the MSR and SR test data. Therefore, we see the modified SLS model proposed in Chapter 6 is able to effectively simulate the stress in the SEC patch under various loading conditions.

7.3 Impact of the Patch Stiffness

Two kinds of patches with different stiffness's, due to different proportions of the Titanium dioxide mixed with the SEBS during fabrication of the elastomer (elastomer is sandwiched between carbon black electrodes), are utilized in the proposed experimental scheme to investigate the impact of patch stiffness on the resultant stress response. It is observed the resultant stress response is more nonlinear in flexible patches than in the stiff patches. Comparative plots were constructed to understand the effect of patch stiffness at a slow loading rate of 0.005 mm/s, moderate loading rate of 0.01 mm/s, and a high loading rate of 0.1 mm/s as shown in Figure 7-4. It can be seen a similar behavioral difference is observed between the stiffer and flexible patches at all three rates of loading. This proves the point the stress response is more nonlinear in flexible patches irrespective to the applied rate of loading.

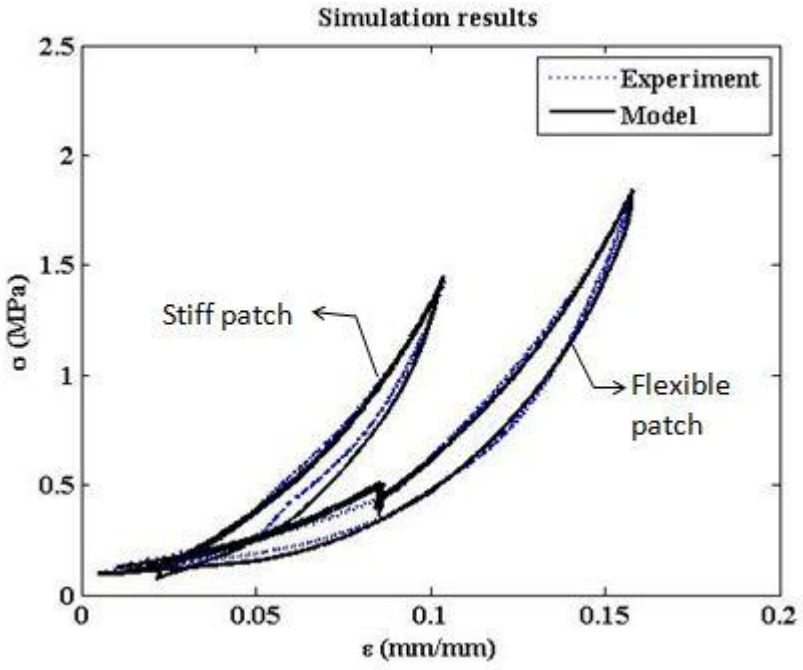

a)

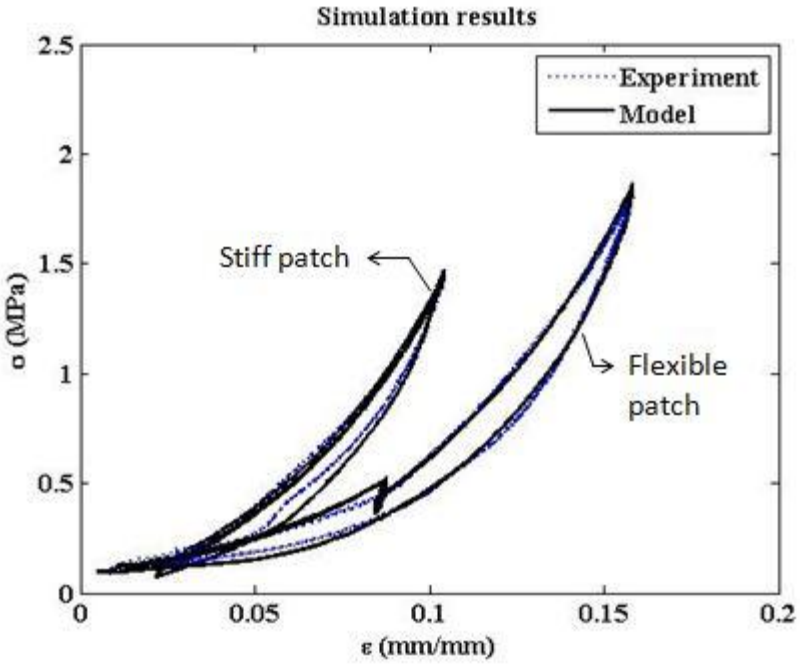

b)

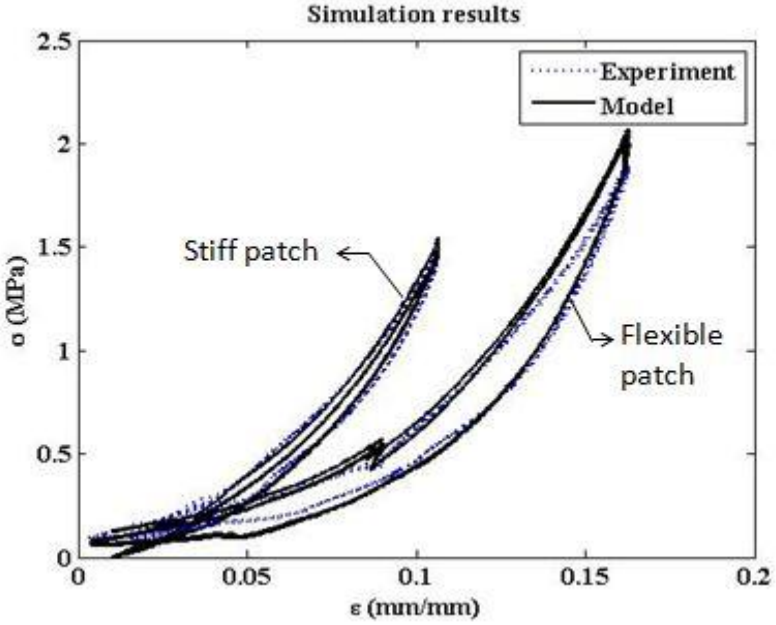

c)

Figure 7-4 : Comparison of resultant stress response under cyclic compression loading a) slow loading rate b) moderate loading rate c) high loading rate.

The resultant stress response can be compared using the parameters tabulated in Table 6-1 and Table 6-2. By investigating the evaluated parameters, the following conclusions are drawn.

- Parameters for the slider remain constant, indicating that quantitatively the equilibrium hysteresis is not dependent on patch stiffness.
- Significant variation is observed in the viscosity parameters, both the power parameter K2 and the switching parameter K1 are dependent on patch stiffness. It can be concluded from the evaluated parameters that the stiffer patch has significantly more stress relaxation than the flexible patch, which physically makes sense. Therefore, the damping/viscous properties are directly related to the patch stiffness; stiffer the patch, the higher the relaxation.
- As shown in Figure 7-4, there is a high nonlinearity in the stress response associated with the flexible patch compared to the stiff patch. It can also be concluded from the elastic parameters (C1, C2 and C3) in Table 6-1 that the nonlinearity in equilibrium response is inversely dependent on patch stiffness—as the stiffness increases, C3 decreases and C1 increases. Owing to the increase in nonlinear behavior, the instantaneous response parameter, also termed as linear elastic spring constant D, decreases with an increase in stiffness.

Finally, it can be concluded for an amount of strain applied on the patch, the flexible patch will have significantly less stress associated with it, when compared to the stiffer patch. Absolute maximum error between the stress predicted from the model and experimental recorded stress is calculated and tabulated below.

Table 7-1: Absolute error in predicted stress response using model – stiff patch

Strain rate	Error value
0.001 mm/s	0.0874 MPa
0.0025 mm/s	0.0836 MPa
0.005 mm/s	0.0878 MPa
0.01 mm/s	0.0872 MPa
0.1 mms	0.101 MPa
0.25 mm/s	0.1347 MPa
0.5 mm/s	0.2243 MPa

Table 7-2 : Absolute error in predicted stress response using model – flexible patch

Strain rate	Error value
0.005 mm/s	0.0876 MPa
0.0075 mm/s	0.0969 MPa
0.01 mm/s	0.0801 MPa
0.05 mms	0.122 MPa
0.1 mm/s	0.176 MPa
0.15 mm/s	0.188 MPa

Maximum stress recorded while testing the stiffer patch in cyclic compression is equal to 1.5 MPa and flexible patch is equal to 1.9 MPa. The comparison indicates that the model is able to effectively reproduce the experimental recorded stress data of both stiff and flexible patches, however slightly better performance is seen in terms of the flexible patches when compared to the stiffer patch. It is observed that there is a little inadequacy in representing the stress-strain response at a low strain level (up to strain level 0.02).

CHAPTER 8. CONCLUSIONS

This thesis summarizes a study conducted to investigate the applicability of a soft elastomeric capacitor as a Weigh-in-Motion sensor. Current state-of-the-art WIM systems are studied to understand their drawbacks and limitations in weight measurement. A soft elastomeric capacitor is introduced and the guiding principle is explained. An experimental scheme is proposed to study the mechanical behavior of the SEC patch under applied compressive strain controlled loading. Several complex models are studied to model the observed resultant stress response of the SEC patch. However, a simple, easy to invert Standard Linear Solid model (SLS) is chosen and modified to model the stress-strain response of the SEC patch for engineering applications.

Three types of tests—multi step relaxation, simple relaxation, and cyclic compression tests—are performed to understand the mechanical behavior of the SEC. MSR test data are used to asymptotically identify the equilibrium response of the SEC patch. By using the loading regime of the simple relaxation test data, the neighborhood of the instantaneous response of the SEC patch can be approximately identified. Rate-dependent behavior for the SEC can be obtained from the stress relaxation data of the simple relaxation tests and multi step relaxation tests. Rate dependence can also be observed in the loading and unloading of the MSR test data and the CC test data. Using these experimental results, a physical model is developed by modifying the standard SLS/Zener model. A slider is added in parallel with the nonlinear spring to construct the equilibrium hysteresis response.

This model can effectively reproduce the equilibrium response of the SEC patch. After evaluating the elastic parameters of the model using the equilibrium response and instantaneous response, viscosity parameters are evaluated using the unconstrained least squares optimization technique by minimizing the error between simulated stress response of the model and the resultant stress response obtained from the experimental data. Comparison is achieved between the simulated stress response and the experimental

data under cyclic compression loading conditions. Results show the model is capable to effectively predict the mechanical behavior of the patch with an average RMS error value approximately equal to 0.11. This permits the use of the model in WIM applications to adequately predict the weight of the vehicle, based on the strain measured in the SEC patch installed under the pavement. Comparison is also completed to investigate the impact of the patch stiffness on the resultant stress response of the SEC patch. It is observed the amount of stress relaxation is directly proportional to the patch stiffness, while the nonlinearity in stress-strain behavior is inversely proportional to the patch stiffness. The proposed model also permits overcoming limitations due to complexities in inverting the model. However, the present work has suggested the model can be improved for predicting the resultant stress response at higher loading rates.

8.1 Applications

The flexible patches compare better against the stiff patches for the Weigh-In-Motion applications. Resultant stress response is found to be smoother independent of the applied loading rate for flexible patches against stiff patches. This can be a potential advantage in the WIM applications. In addition to that, the results shown in Table 7-1and Table 7-2 indicate that the model is able to effectively reproduce the mechanical behavior of the flexible SEC patch with better accuracy over stiff SEC patch. Therefore the present work has suggested for considering the flexible patches to be installed under the pavements for WIM applications. Prediction capabilities of the model can be further improved by considering environmental factors like temperature. It will be the main interest in developing a fully function SEC based Weigh-In-Motion system.

8.2 Scope for Further Research

The modified standard linear solid model is well capable of predicting the mechanical behavior of the SEC patch. However, results and observations furnished herein can be extended further as mentioned below.

- Improved experimental test setup can be employed for using more than one LVDT to measure the axial displacement of the SEC patch. Average axial displacement can be considered to reduce the dynamic effects of the actuator controlled by hydraulics during tests conducted at high loading rates. This would reduce the noise in the recorded strain data and improve the accuracy of the model to predict the mechanical behavior of the SEC patch.
- Model prediction can be improved further by investigating the effect of environment conditions like temperature, humidity, etc. Fatigue response from the SEC patch can be investigated to observe the resultant stress response of the patch after several hundreds of tests are performed.
- A soft elastomeric capacitor can be connected to a data acquisition system, while the experiment is performed to record the capacitance. These data can be used to evaluate a mathematical relationship between the measured capacitance to the applied loading.
- An array of SEC patches can be installed under a pavement in a laboratory environment or in real traffic at controlled/low speeds to test the predicting capabilities of the model and can be further improved, based upon the observations. An algorithm can be developed to estimate the vehicular weight, speed, and location, using an array of sensors.

REFERENCES

Amin, A.F.M.S., M.S. Alam, and Y. Okui. "An improved hyperelasticity relation in modeling viscoelasticity response of natural and high damping rubbers in compression: experiments, parameter identification and numerical verification." *Mechanics of materials*, 2002: 75-95.

Arruda, E.M., M.C. Boyce, and Jayachandran.R. "Effects of strain rate, temperature and thermomechanical coupling on the finite strain deformation of glassy polymers." *Mechanics of Materials*, 1995.

ASTM International. "Standard specification for Highway WIM systems with user requirements and test methods." West Conshohocken, PA., 2009.

Bardenhagen, S., M. Stout, and G. Gray. "Three dimensional, finite deformation, viscoplastic constitutive models for polymeric materials." *Mechanics of materials*, 1997: 235-253.

Bergan, A.T., C.F. Berthelot, and B. and Taylor. "Effect of Weigh in Motion Accuracy on Weight enforcement accuracy." Annuam meeting of ITS- America, 1997.

Bergstom, J.S. "Constitutive Modeling of Elastomers – Accuracy of Predictions and Numerical Efficiency." *polymerfem.com.* 2003. http://polymerfem.com/polymer_files/Elastomer_Modeling_Comparison.pdf.

Bergstrom, J.S., and M.C. Boyce. "Large strain time- dependent behavior of filled elastomers." *Mechanics and materials*, 2001: 627-644.

Bhuiyan, A., Y. Okui, H. Mitamura, and T. Imai. "A rheology model of high damping rubber bearings for seismic analysis:Identification of nonlinear viscosity." *International Journal of Solids and Structures*, 2009: 1778-1792.

Blumenthal, W.R., and C.M. Cady. "Infulence of temperature and strain rate on compressive behavior of PMMA and polycarbonate polymers." *American Institute of Physics.* Newyork, 2002.

Boyce, M.C., and E.M. Arruda. "Constitutive modeling of the large strain time-dependent behaviourof elastomers." *Rubber Chemistry Technology*, 2000: 504-523.

Boyce, M.C., S. Socrate, and P.G. Llana. "Constitutive model for the finite deformation stress–strain behavior of poly(ethyleneterephthalate) above the glass transition." *Polymer*, 2000: 2183-2201.

Brinson, H.F., and L.C Brinson. "Differential constituive equations." In *Polymer engineering science and viscoelasticity*, by H.F. Brinson and L.C Brinson. Springer, 2008.

Brinson, H.F., and L.C. Brinson. *Polymer Engineering science and Viscoelasticity- An Introduction.* Springer, 2008.

Bueche, F. "Mullins effect and rubber-filler interaction." *Applied polymer science*, 1961: 271-281.

Bushman, R., and J.P. Andrew. "Weigh in motion technology - Economic ans performance." Charlotte: NATMEC, 1998.

Chang, C., and M. Rahul. "Fiber optic sensors for transportation infrastructural health monitoring." *American journal of engineering and applied sciences*, 2010: 214-221.

Chatterjee, P., E. O'Brien, T. Li, and A. and Gonzalez. "Wavelet domain analysis for identification of vehicle axles from bridge measurements." *Computers and structures* 84 (2006): 1792-1801.

CTRE - ISU, Center for transportation research and education. *State's successful practices weigh-in-motion handbook.* Federal Highway Administration, 1997.

Davis, Stacy C., and Diegel W . Susan. *Transportation Energy Data Book.* Tennesse: Center for Transportation Analysis, 2002.

Diani, J., B. Fayolle, and P. Gilormini. "A review on the Mullins effect." *European polymer journal*, 2008.

Drozdov, A.D., and J.deC. Christiansen. "Modeling the viscoplatic response of polyethylene in uniaxial loading–unloading tests." *Mechanics Research Communications*, 2003: 431-442.

European Commission. *Weigh-in-motion of axles and vehicles for Europe (WAVE).* Laboratorie Central des Ponts et Chausseess, 2001.

Global, IPC. *Universal testing machines - UTM 25.* 2013. http://www.ipcglobal.com.au/products/product-range/utm-25.html.

Gonzalez, A, C Rowley, and E.J and OBrien. "A general solution to the identification of moving vehicle forces on a bridge." *International journal for numerical methods in engineering*, 2008.

Groenendijk, J., C.H. Vogelzang, A. A. A. Molenaar, B. R. Mante, and L. J. M. Dohmen. "Linear Tracking Response Measurements: Determining Effects of Wheel-Load Configurations." *Transportation Research Board*, 1997.

Hann, Y.M., and G.M. Sluimer. "Standard linear solid model for dynamic and time-dependent behavior of building materials." *Heron*, 2001.

Harwood, J.A.C., L. Mullins, and A.R. and Payne. "Stress softening in natural rubber vulcanizates." *Journal of Applied Polymer Science*, 1965.

Jacob, B, and Feypell-de la Beaumelle. "Improving truck safety : Potential of weigh-in-motion technology." *IATSS Research*, 2010: 9-15.

Khan, A., and H. Zhang. "Finite deformation of a polymer: experiments and modeling." *International Journal of Plasticity*, 2001: 1167-1188.

Khan, A.S., and R. Liang. "Behavior of three BCC metal over a wide range of strain rates and temperatures." *International journal of plasticity*, 1999.

Kim, O.K., C.A. Bell, and J.E. Wilson. "Effect of Increased Truck Tire Pressure on Asphalt Concrete Pavements." *Journal of Transportation Engineering*, 1989.

Kistler Instrumente AG. "The first system for monitoring at any speed." Switzerland, 1997.

Kollosche, M, H Stoyanov, and S and Kofod, G Laflamme. "Strongly enhanced sensitivity in elastic capacitive strain sensors." *Journal of materials chemistry*, 2011.

Krempl, E., and F. Khan. "Rate (time)-dependent deformation behavior: an overview of some properties of metals and solid polymers." *International Journal of Plasticity*, 2003: 1069-1095.

Laflamme, S., M. Kollosche, J.J. Connor, and G. and Kofod. "Robust flexible capacitive surface sensor for structural health monitoring applications." *ASCE Journal of Engineering Mechanics*, 2012.

Laflamme, S., M. Kollosche, J.J. Connor, and G. Kofod. "Large scale capacitance sensor for health monitoring of civil structures." *Structural control and monitoring.* 2010.

Laflamme, S., M. Kollosche, J.J. Connor, and G. Kofod. "Soft capacitive sensor for structural health monitoring of large-scale systems." *Structural Control and Health Monitoring*, 2010: 70-81.

Laflamme, S., M. Kollosche, V.D. Kollipara, H.S. Saleem, and G. and Kofod. "Large scale surface strain gauge for health monitoring of civil structures." *SPIE.* 2012.

Linjun, Y, M Fraser, A Elgamal, T Fountain, and K and Oliver. "Neural networks and Principal component analysis for strain-based vehicle classification." *ASCE Journal of computing in civil engineering*, 2008.

Luz Elena, Y.M, and A.K Lawrence. *Summary of vehicle detection and survelliance technologies used in intelligent transportation systems.* Federal highway administration, 2000.

Mooney, M. "A theory of large elastic deformation." *Applied Physics*, 1940.

Moses, F. "Weigh-in-motion system using instrumented bridges." *ASCE Transportation engineering journal* 105 (1979): 233-249.

Mullins, L. "Softening of rubber by deformation." *Rubber Chem Technol*, 1969.

Murali Krishnan, J., and K. Rajagopal. "Thermodynamic Framework for the Constitutive Modeling of Asphalt Concrete: Theory and Applications." *Journal of Materials in Civil Engineering*, 2004: 155-166.

Navarrette, M.C, and E Bernabeu. "Fibre-optic weigh-in-motion sensor." *Sensors and actuators*, 1994: 110-113.

Nyman, W, and F and Moses. "Calibration of bridge fatigue design model." *Journal of structural engineering* 111 (1985): 1251-1266.

O'Brien, E, A Znidaric, and A and Dempsey. "Comparison of two independently developed bridge weigh-in-motion systems." *International journal of vehicle design, Heavy vehicle systems* 6 (1999): 147-161.

Peters, R.J. "An unmanned and undetectable highway speed vehicle weighing system." AARB conference proceedings, 1986.

Richeton, J., S. Ahzi, K.S. Vecchio, F.C. Jiang, and R.R Adharapurapu. "Influence of temperature and strain rate on the mechanical behavior of three amorphous polymers." *International journal of Solids and Structures*, 2005.

Rivlin, R.S. "Large elastic deformations of isotropic materials VII. Experiments on the deformation of rubber." *Phil. Trans. Roy. Soc.*, 1951.

Saber, Aziz, and Freddy Roberts. "Economic Impact of Higher Tuck Loads on Remaining Safe Life of Lousiana Bridges." *Transportation Research Board Annual Meeting.* TRB, 2006.

Saleem, H.S., T. Mahendra, M. Kollosche, M. Kessler, and S. Laflamme. "Bio-Inspired Sensory Membrane: Fabrication Processes for Full-Scale Implementation." *Quantitative Nondestructive evaluation.* Denver, CO, 2012.

Scheuter. "Sources of error in dynamic weight measurement." *Traffic technology international magazine*, 1997: P1215 - (E0-E4).

Scheuter, F. "Evaluation of factors affecting WIM system accuracy." Lisbon: Proceedings of 2nd European conference on WIM, 1998.

Siddharthan, R., N. Krishnamenon, M. El-Mously, and P. Sebaaly. "Investigation of Tire Contact Stress Distributions on Pavement Response." *Journal of Transportation Engineering*, 2002: 136-144.

Swan, L, and C and Fairfield. "The dynamic response of the Berwick- Upon-Tweed bypass bridge." *Insigiht- Nondestructive testing and condition monitoring* 50 (2008): 35-41.

Wang, Jinfang, and Mingguang Wu. "An Overview of Research on Weigh- in-motion System." *World Congress on Intelligent Control and Automation.* 2004.

Wang, T.L.,, and C., Liu. *Influence of Heavy Trucks on Highway Bridges.* Florida Department of Transportation, 2000.

Wei, C, C Chang, and S and Wang. "Vehicle classification using advanced techniques." *Transportation research record* 1551 (1996): 45-50.

Yeoh, O.H. "Some forms of the strain energy function for rubber." *Rubber chemistry and technology*, 1993.

Zhong, Q.Y., and J.S. Otto. "Effects of tire - pavement contact pressure distributions on the response of asphalt concrete pavements." *Canadian Journal of Civil engineering*, 1995.